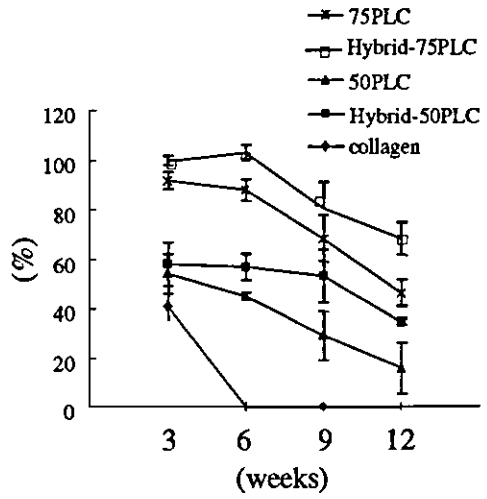

Fig. 2. The remaining masses of the scaffolds were determined at the indicated time points. ((a) hybrid-75PLC scaffold, (b) 75PLC scaffold, (c) hybrid-50PLC scaffold, (d) 50PLC scaffold, and (e) collagen scaffold).

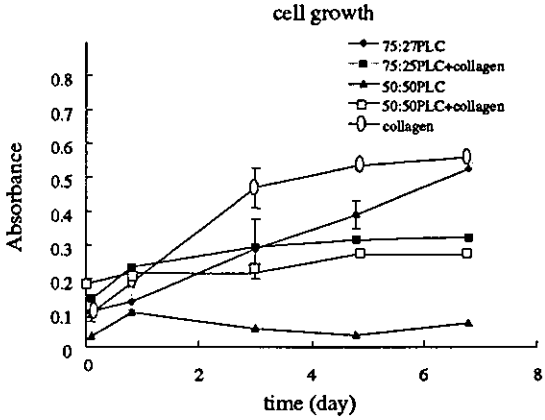

Fig. 3. Cell growth levels were determined at the indicated time points. The data show that the MTT was directly proportional to the number of cells.

(7 days), while the number of cells on the hybrid-50PLC and the hybrid-75PLC continued to grow relatively smaller. The 5-fold expansion of chondrocytes on the 75PLC after the 7 days of incubation was also greater than the 3-fold expansion on the hybrid-75PLC. The chondrocytes proliferated faster on the collagen scaffold compared to the other scaffolds.

3.3. *Fluorescent microscopy*

Figs. 4(a–o) show all pores have continuous linkages in all scaffolds. The cells uniformly invaded and attached to scaffolds with pore sizes around 200 μm. It was found that cells attached to the scaffolds coated with collagen more than to other non-coated scaffold after 24-h incubation. This phenomenon was prominent with the 50PLC. The cells grew along the surface of the scaffold and these cells were found to connect with one other on all of the scaffolds except for the 50PLC. Cells were found to float in the 50PLC rather than attaching. Cells on all scaffolds, except the 50PLC, had similar sizes and shapes. The cells grown on the scaffolds were found to cover the entire scaffold after 7 days of incubation. However, when the 50PLC was applied as a chondrocyte scaffold, the growth of cells was not found after a 7-day incubation. With the 7-day incubation, no extracellular matrix around the cultured cells was found on any of the scaffolds.

3.4. *SEM analysis*

The interaction between the chondrocytes and the scaffolds was characterized morphologically and chondrocytes were visualized by SEM. Chondrocytes on every scaffold maintained their round shape after 24-h incubation, as shown in Figs. 5(a–c). The chondrocytes maintained a spherical chondroblastic shape. No difference with respect to chondrocyte morphology was seen among the 75PLC, the 50PLC and the collagen scaffold at 24 h posts seeding.

3.5. *Cartilage formation in vivo*

Primary chondrocytes at pre-confluence were collected as a cell suspension and inoculated into the scaffolds as described in the Methods section. CSCs thus prepared were subcutaneously implanted into nude mice. After 4-week implantation, gross observations suggested that the implanted CSCs had formed a solid, whitish-yellow surface, and could be easily separated from the surrounding tissues, consistent with a previous report [12]. The CSCs maintained the exact dimensions of the original scaffold. Similar results were obtained in 6-month in vivo studies using rat costal chondrocytes immersed on PLCs (data not shown). However, the volume of the collagen scaffold was 50% decreased compared to the original volume. With respect to shape retention, the dimensions demonstrated significant variability between the PLCs and the collagen scaffold.

In all the scaffolds, no inflammatory signs were observed in the implanted regions throughout the implanted period. Cartilage-like tissue was present in all scaffolds inoculating primary chondrocytes after 4-week implantation. The extracellular matrix around cells was stained with alcian blue suggesting an abundant accumulation of S-GAG contents (Figs. 6a–c). The cartilage formation area in the 75PLC was generally greater than that of the 50PLC. However, there was no significant difference in the amount of cartilage tissue area among all groups tested, regardless of scaffolds (in preparation). No scaffolds without cells (negative controls) showed positive tissue at 4 weeks; only loose fibrous tissue was present in the scaffold.

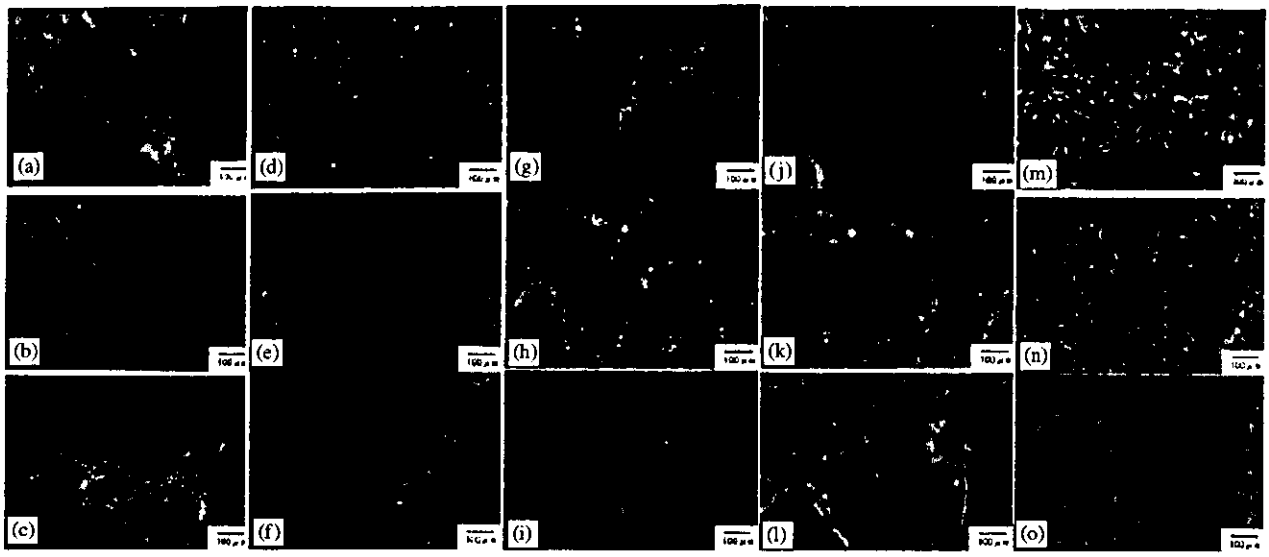

Fig. 4. Fluorescence microscopic observation. (a), (d), (g), (j), (m)—day 1. (b), (e), (h), (k), (n)—day 4. (c), (f), (i), (l), (o)—day 7. (a–c)—75PLC scaffold, (d–f)—hybrid-75PLC scaffold, (g–i)—50PLC scaffold, (j–l)—hybrid-50PLC scaffold, and (m–o)—collagen scaffold.

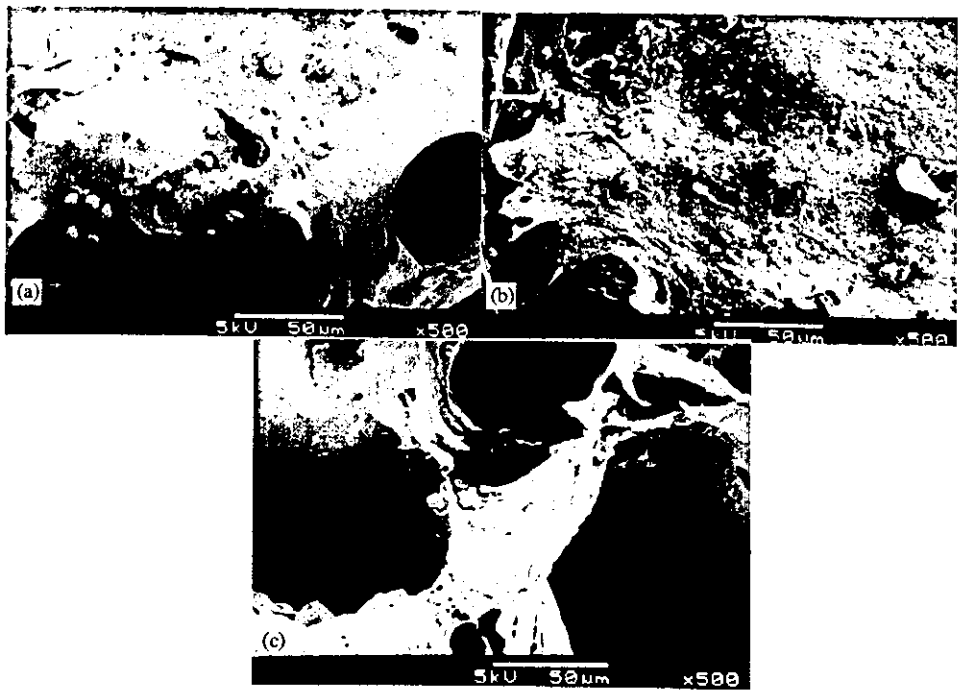

Fig. 5. SEM demonstrating round cell-like chondrocytes at day 1 p.o. Chondrocytes on all the scaffolds show the typical polygonal pattern. (a) 75PLC scaffold, (b) 50PLC scaffold, and (c) collagen scaffold.

4. Discussion

A recent study by our group showed that the 50PLC is useful for creating a scaffold for chondrocytes in vivo [12]. PLC scaffolds have been implanted successfully as nerve guides and were found to be non-toxic with a minor foreign-body reaction [22–24]. Very little is known, however, about how the PLC can be used for phenotypic expression of chondrocytes [11]. The present study expands upon previous work, and revealed adhesion, proliferation, and morphology of costochondral resting zone chondrocytes on the PLC scaffolds in vitro. Additionally, we compared PLC and collagen scaffolds, and also utilized a preparation of PLC coated with type I collagen (hybrid-PLC). Collagen scaffolds are well studied for a variety of cells [2,25,26] and have

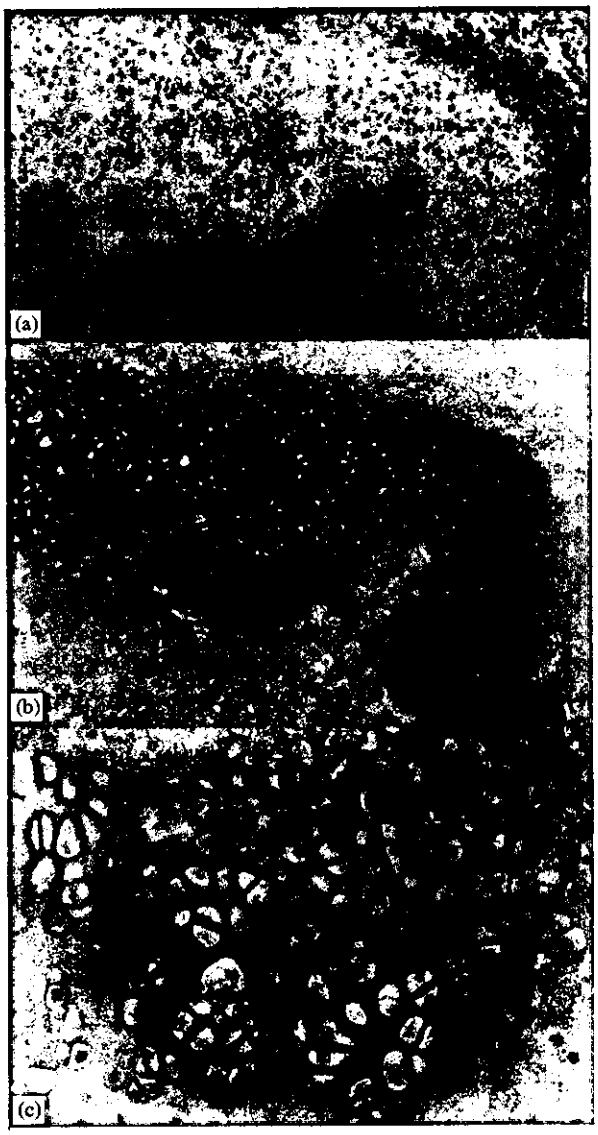

Fig. 6. Cartilage formation in vivo histology of grafted rat chondrocytes 4-weeks post-implantation demonstrating developing cartilage and cell clusters within a PCL sponge; H&E, 100× magnification. (a) Typical hyaline cartilage formation with HE staining, (b) the extracellular matrix around the cells was stained with alcian blue, and (c) high magnification of Fig. 6b.

been found to have the proper molecular cues to stimulate new collagen production by implanted cells as compared with PGA non-woven fabrics [25]. Ben-Yishay et al. showed that the defects grafted with cell-seeded collagen scaffold demonstrated enhanced healing at all time points [26]. An in vitro test system is suitable for the assessment of the materials because it shows that cultured cells survive in contact with the test materials [27]. An ideal biodegradable polymer scaffold for chondrocytes should be biocompatible, promote attachment and proliferation, maintain the phenotype and activity of cells, have an adequate degradation rate, and, in consequence, allow successful cartilage regeneration.

The experimental design compared the effects of the polymer surface on the morphology of the cells. SEM analysis was used to visualize chondrocytes. It is well known that chondrocytes maintain a spherical morphology with reduced interaction between the cells and extracellular matrix, which is indicative of the expression of a differentiated phenotype (Figs. 5a–e) [28,29]. There was no significant difference in their morphologic appearance between the PLC and the collagen scaffold which may indicate a trigger of differentiation and stimulation of the synthesis of tissue-specific collagen type II [30]. From these results, the PLC sponges are clearly biocompatible materials that, as shown in this study, can maintain the phenotype of chondrocytes.

The 75PLC, the 50PLC, and the collagen scaffolds were characterized by the presence of two distinct cellular morphologies under fluorescence microscopy (Fig. 4). In the 75PLC and the collagen scaffolds, chondrocytes that were directly attached to the scaffold assumed a spindle shape. However, cells which were not attached to the 50PLC were spherical in shape and thus resembled typical chondrocytes. This may explain why the growth of cells on the 50PLC was not found 7 days after culture. The cells on the 50PLC may not have been able to disrupt growth because they did not attach to the 50PLC. Therefore, this suggests that the difference in chondrocyte growth between the 75PLC and the 50PLC is due to differences in the PLC surface characteristics. The generally accepted idea is that the absorption of serum proteins is a factor [11,31,32], which may also explain the difference. The 75PLC may have absorbed more adhesional factor than the 50PLC surface, thus conserving the extracellular matrix [33,34]. The ability to bind and support the differentiation of chondrocytes makes the hybrid-75PLC, like the collagen scaffold, a good candidate for a scaffold in models of tissue-engineered cartilage. The increase in cell attachment induced by pre-treatment of the scaffold with collagen suggested an integrin or fibronectin-mediated mechanism [35]. However, there were no differences in cell growth between the hybrid-75PLC and hybrid-50PLC, while cell growth on the 75PLC was superior to that of the 50PLC. From these results, both collagen-coated PLCs are likely to have similar cell modality characteristics. It is concluded that the surface of the PLC itself has a strong effect on cell growth. However, there was a difference in cell growth between the collagen-coated PLCs and the collagen scaffold. This suggests that there are different characteristics between the surfaces of collagen-coated hybrid-PLCs and collagen scaffold.

The absorption period of the collagen-coated PLCs was slower than that of the non-coated PLCs. This is

because the thickness of the sponge increased due to the collagen solution coating around the PLC.

To examine the possibilities of using these scaffolds for tissue-engineered cartilage, two series of hybrid-PLCs and the collagen scaffold, respectively, were implanted. The pore size of all the scaffolds used in this study was similar at approximately 100–200 μm. Cartilage tissue was present in all scaffolds containing chondrocytes after 4 weeks of implantation. Gross examination of the composites, however, revealed differences among the PLCs and the collagen scaffold. The volume of the collagen scaffold after a 4-week implantation was 50% of the original volume. The PLC composites maintained the exact dimensions of the original polymer scaffold. Similar results were obtained after 6 months using the PLC materials (data not shown). According to Solchaga et al. [35], as a result of rapid degradation of reabsorption in vivo, an ACP sponge based on hyaluronic acid cannot be recovered after implantation. Since cartilage tissue is formed after a certain generation time, the degradation rate of the polymer should not be too fast. A recent study reported that the shape of PLG-H implants (80 wt% 75:25PLG+20 wt% 75:25PLG) changed, whereas the shape of PLG-FR (fiber-reinforced) implants did not [36]. The difference found in the gross observation between the PLCs and the collagen scaffold can be explained by the difference in the degradable period of these materials [36]. The previous study reported that the collagen scaffold was not a viable scaffold for chondrocytes to form cartilage tissue [12]. Collagen scaffold is biodegradable and the turnover rate is relatively high; in fact, the degradation rate of the collagen scaffold was too high for subcutaneous location in nude mice; the collagen scaffold had completely degraded after 2 weeks in a previous report [12]. Therefore, in this study, an improved collagen scaffold was used to delay the degradation time by adding cross-links using dehydrothermal treatment or UV irradiation. The biodegradation rate of collagen-based implants is known to be strongly affected by the cross-linking density [37–39]. Cross-linking can also improve the tensile properties of the materials to such a level that they are handled and sutured with ease [40]. The results of this study further demonstrate the importance of material substrates for tissue-engineered cartilage. As previously mentioned, the susceptibility of polymers to degradation is of increasing importance in the selection and application of scaffolds, especially for chondrocytes. Although the optimal degradation period has not yet been established, our preliminary results suggest that the choice of an appropriate period is necessary; 1 month or more is essential for a cartilage graft. Since the scaffolds act as a temporary matrix around the cells, it is critical to understand the degradation behavior.

5. Conclusion

The 75:25 PLC sponge tested in this experiment was more efficient than the other PLC sponges with respect to the number of cells grown per unit volume of scaffold. The PLC sponge coated with collagen also proved to be superior to the non-coated PLC sponge in terms of the number of cell attachments.

Cartilage tissue was formed subcutaneously using chondrocytes and all the biodegradable polymers. However, the collagen scaffold with chondrocytes did not maintain its original shape when the chondrocyte composites and collagen scaffolds were sampled 4 weeks after grafting. These features make the 75:25PLC sponge an excellent candidate for use as a scaffold for chondrocytes in tissue-engineered cartilage.

Future experiments will investigate the feasibility of this newly formed cartilage for the repair of maxillofacial cartilage defects. Experiments will focus on how to faster regenerate the cartilage tissue more quickly from the isolated cells, graft–host interaction and the durability of the newly formed cartilage after intramaxillofacial implantation. The long-term goals of this work are to create cartilage tissue with clinically appropriate form and function.

Acknowledgements

This work was supported in part of by Grant-in-aid for University and Society Collaboration (KAKENHI:12794015). We also thank Dr. Yoshito Ikada, Institute for Frontier Medical Sciences, Kyoto University, for valuable comments and suggestion.

References

[1] Vacanti CA, Langer R, Schloo B, Vacanti JP. Synthetic polymers seeded with chondrocytes provide a template for new cartiage formation. Plast Reconstr Surg 1991;88:753–9.
[2] Fujisato T, Sajiki T, Liu Q, Ikada Y. Effect of basic fibroblast growth factor on cartilage regeneration in chondrocyte-seeded collagen sponge scaffold. Biomaterials 1996;17:155–62.
[3] Freed LE, Hollander AP, Martin I, Barry JR, Langer R, Vunjak-Novakovic G. Chondrogenesis in a cell–polymer–bioreactor system. Exp Cell Res 1998;240:58–65.
[4] Freed LE, Marquis JC, Nohria A, Emmanual J, Mikos AG, Langer R. Neocartilage formation in vitro and in vivo using cells cultured on synthetic biodegradable polymers. J Biomed Mater Res 1993;27:11–23.
[5] Chu CR, Dounchis JS, Yoshioka M, Sah RL, Coutts RD, Amiel D. Osteochondral repaire using periochondrial cells A 1-year study in rabbits. Clin Orthop 1997;340:220–9.
[6] Sittinger M, Reitzel D, Dauner M, Hierlemann H, Hammer C, Kastenbauer E, Planck H, Burmester GR, Bujia J. Resorbable polyesters in cartilage engineering: affinity and biocompatibility of polymer fiber structures to chondrocytes. J Biomed Mater Res 1996;33:57–63.

[7] Freed LE, Grande DA, Lingbin Z, Emmanual J, Marquis JC, Langer R. Joint resurfacing using allograft chondrocytes and synthetic biodegradable polymer scaffolds. J Biomed Mater Res 1994;28:891–9.
[8] Freed LE, Vunjak-Novakovic G, Biron RJ, Eagles DB, Lesnoy DC, Barlow SK, Langer R. Biodegradable polymer scaffolds for tissue engineering. Biotechnology (NY) 1994;12:689–93.
[9] Ma PX, Schloo B, Mooney D, Langer R. Development of biomechanical properties and morphogenesis of in vitro tissue engineered cartilage. J Biomed Mater Res 1995;29:1587–95.
[10] Minuth WW, Sittinger M, Kloth S. Tissue engineering: generation of differentiated artificial tissues for biomedical applications. Cell Tissue Res 1998;291:1–11.
[11] Ishaug SL, Okun LE, Prado G, Applegate MA, Ratcliffe A. Human articular chondrocytes adhesion and proliferation on synthetic biodegaradable polymer films. Biomaterials 1999;20: 2245–56.
[12] Honda M, Yada T, Ueda M, Kimata K. Cartilage formation by cultured chondrocytes in a new scaffold made of poly (L-lactide-ε-caprolactone) sponge. J Oral Maxillofac Surg 2000;58:767–75.
[13] Matsui T, Nakamura T, Tsuda T, Ikada Y. Bioabsorption of poly caprolactone and copolymer of ε-caprolactone and L-lactide. J Jpn Soc Biomater 1993;11:330–9.
[14] Nakayama A, Kawasaki N, Yamamoto N. Enzymatic hydrolysis of poly (L-lactide-co-ε-caprolactone)s. Jpn SEN-I GAKKAISHI 1995;15:131–9.
[15] Hyon SH, Nakamura T, Cha WI. Synthesis and properties of elastomeric lactide–caprolactone copolymers. Jpn J Biomater 1996;14:223–31.
[16] Perego G, Cella GD, Aldini NN, Fini M, Giardino R. Preparation of a new guide from a poly (L-lactide-co-6-caprolactone). Biomaterials 1994;15:189–96.
[17] de Groot JH, Zijlstra FM, Kuipers HW, Pennings AJ, Klompmaker J, Veth RPH, Jansen HWB. Meniscal tissue regeneration in porous 50/50 copolymer (L-lactide/ε-caprolactone) implants. Biomaterials 1997;18:613–22.
[18] Grande DA, Schwartz RE, Zhou L, Kwan M. The durability and biomechanical properties of chondrocyte/collagen allografts. Trans Orthop Res Soc 1993;18:731–9.
[19] Shinomura Y, Yoneda T, Suzuki F. Osteogenesis by chondrocytes from growth cartilage of rat rib. Calcif Tissue Res 1975;19:179–87.
[20] Mosmann T. Rapid colorimetric assay for cellular growth and survival: application to proliferation and cytotoxicity assays. J Immunol Meth 1983;65:55–63.
[21] Periasamy N, Armiji M, Verkman AS. Picosecond rotation of small polar fluorophores in the cytosol of sea urchin eggs. Biochemistry 1991;30:11836–41.
[22] den Dunnen WFA, Schakenraad JM, Zondervan GJ, Pennings AJ, van der Lei B, Robinson PH. A new PLLA/PCL copolymer for nerve regenaration. J Mater Sci Mater Med 1993;4:521–5.
[23] den Dunnen WFA, van der Lei B, Schakenraad JM, et al. Long term evaluation of nerve regeneration in a biodegradable nerve guide. Microsurgery 1993;14:508–15.
[24] den Dunnen WFA, van der Lei B, Robinson PHA, Holwerda A, Pennings AJ, Schakenraad JM. Biological perfomance of a degradable poly(lactic acid-ε-caprolactone) nerve guide; influence of tube dimensions. J Biomed Mater Res 1995;29: 757–66.
[25] Grande DA, Halberstadt C, Naughton R, Schwartz R, Manji R. Evaluation of matrix scaffolds for tissue engineering of articular cartilage grafts. J Biomed Mater Res 1997;34:211–20.
[26] Ben-Yishay DA, Grande MI, Pitman DM. Repair articular cartilage defects using collagen–chondrocyte allograft. Trans Orthop Res Soc 1992;17:174.
[27] Loty S, Sautier JM, Loty C, Boulekbache H, Kokubo T, Forest N. Cartilage formation by fetal rat chondrocytes cultured in alginate beads: a proposed model for investigating tissue–biomaterial interaction. J Biomed Mater Res 1998;42:213–22.
[28] von der Mark K, Gauss V, von der Mark H, Muller P. Relationship between cell shape and type of collagen synthesized as chondrocytes lose their cartilage phenotype in culture. Nature 1977;267:531–2.
[29] Solursh M. Formation of cartilage tissue in vitro. J Cell Biochem 1991;45:258–60.
[30] Benya D, Shaffer J. Dedifferentiated chondrocytes reexpress the differentiated collagen phenotype when cultured in agarose gels. Cell 1982;30:215–24.
[31] Andrade JD, Hlady V. Protein adsorption and materials biocompatibility: a tutorial review and suggested hypotheses. Adv Polym Sci 1986;79:1–63.
[32] Hambleton J, Schwartz Z, Khare A, Windeler SW, Luna M, Brooks BP, Dean DD, Boyan BD. Culture surfaces coated with various implant materials affect chondrocyte growth and metabolism. J Orthop Res 1994;12:542–52.
[33] Grinell F. Cellular adhesiveness and extracellular substrata. Int Rev Cytol 1978;53:65–144.
[34] Weiss RE, Reddi AH. Appearance of fibronectin during the differentiation of cartilage, bone, and bone marrow. J Cell Biol 1981;88:630–6.
[35] Solchaga LA, Dennis JE, Goldberg VM, Caplan AI. Hyaluronic acid-based polymers as cell carriers for tissue-engineered repair of bone and cartilage. J Orthop Res 1999;17:205–13.
[36] Lohmann CH, Schwartz Z, Niederauer GG, Carnes Jr DL, Dean DD, Boyan BD. Pretreatment with platelet derived growth factor-BB modulates the ability of costochondral resting zone chondrocytes incorporated into PLA/PGA scaffolds to form new cartilage in vivo. Biomaterials 2000;21:49–61.
[37] Weadock K, Olson RM, Silver FH. Evaluation of collagen crosslinking techniques. Biomater Med Dev Art Org 1983; 11:293.
[38] Chvapil M, Owen JA, Clark DS. Effect of collagen crosslinking on the rate of resorption of implanted collagen tubing in rabbitis. J Biomed Mater Res 1977;11:297.
[39] Tomihata K, Burczak K, Shiraki K, Ikada Y. Cross-linking and biodegradation of native and denature collagen, Polymers of biological and biomedical significance. ACS Symposium Series 540, 1994. p. 275–86.
[40] Vacanti CA, Langer R, Schloo B, Vacanti JP. Synthetic polymers seeded with chondrocytes provide a template for a new cartilage formation. Plast Reconstr Surg 1991;88:753–9.

Cartilage Formation by Serial Passaged Cultured Chondrocytes in a New Scaffold: Hybrid 75:25 Poly(L-Lactide-ε-Caprolactone) Sponge

Masaki J. Honda, DDS, PhD, Toshikazu Yada, PhD,† Minoru Ueda, DDS, PhD,‡ and Koji Kimata, PhD§*

Purpose: This study was designed to determine whether multipled chondrocytes immersed in a new scaffold, 75:25 poly(L-lactide-ε-caprolactone) sponge coated with type I collagen (75-PLC scaffold), could be used to generate cartilage tissue in vivo and to evaluate the correlation between cartilage generation and the phenotype of the proliferated chondrocytes.

Materials and Methods: Rat chondrocytes were suspended in 75-PLC scaffold at a density of 1×10^7 cells/mL after proliferation in a monolayer for 1 (P1) to 4 passages (P4) and implanted in nude mice for 4 weeks. Cells were characterized by the expression of genes encoding type II collagen, aggrecan, and type I collagen by Northern hybridization, and consequently, the newly formed tissue was evaluated histologically.

Results: The expression of aggrecan messenger RNA gradually decreased with the passaged cultures; however, the expression of type I collagen messenger RNA increased with time. The cartilage formations in all specimens were found not only in P1 chondrocytes but also in P2 chondrocytes, although when P3 chondrocytes were grafted, approximately 50% of cartilage formation was still observed up to but not beyond P4.

Conclusion: It is suggested that cartilage tissue is generated with cultured chondrocytes up to P2 but not beyond P4. Northern blot analysis is useful for the assessment of whether the cells are capable of regeneration.

J Oral Maxillofac Surg 62:1510-1516, 2004

Tissue engineering is one of the most promising approaches for cartilage repair.[1-5] However, there remain many problems to overcome before tissue-engineered cartilage is used in clinical applications. The question of the selection of suitable cells to engineer cartilage graft material has been problematic because of the scarcity of donor sites and the morbidity associated with surgical harvesting. To solve this problem, the required amount of chondrocytes may be generated by in vitro proliferation of isolated chondrocytes in monolayer cultures.[6,7] However, chondrocytes cultured in monolayers tend to lose their phenotype, as assessed by aggrecan and collagen production, a process called dedifferentiation.[8-10]

In a previous study, a 50:50 poly(L-lactide-ε-caprolactone) sponge was used as a scaffold for tissue-engineered cartilage inoculated with P1 (1 passage) chondrocytes.[11] It was not suitable for regenerating cartilage tissue, because histologic examination revealed the presence of fibrous tissue impregnating the cartilage in the implants. The percentage of fibrous tissue formation in the total cartilage formation was

*Research Associate, Tooth Regeneration Division of Stem Cell Engineering, The Institute of Medical Science, The University of Tokyo, Tokyo, Japan.

†Research Fellow, Institute for Molecular Science of Medicine, Aichi Medical University, Aichi, Japan.

‡Professor and Chairman, Department of Oral and Maxillofacial Surgery, Nagoya University School of Medicine, Nagoya, Japan.

§Professor and Director, Institute for Molecular Science of Medicine, Aichi Medical University, Aichi, Japan.

This work was supported in part by a Grant-in-aid for University and Society Collaboration (KAKENHI:12794015).

Address correspondence and reprint requests to Dr Honda: Tooth Regeneration Division of Stem Cell Engineering, The Institute of Medical Science, The University of Tokyo, 4-6-1 Shirokanedai Minato-ku, Tokyo 108-8639, Japan; e-mail: honda-m@ims.u-tokyo.ac.jp

0278-2391/04/6212-0011$30.00/0
doi:10.1016/j.joms.2003.12.042

35%.[11] We developed an improved biodegradable scaffold; a 75:25 poly(L-lactide-ε-caprolactone) sponge coated with type I collagen (75-PLC scaffold). The new scaffold appears to be superior to other scaffolds used to support chondrocytes.[12] Despite many reports of tissue-engineered cartilage that uses many types of scaffolds, none have considered cell culture to be valuable for subsequent cartilage formation after implantation. The aims of the present study were 1) to determine whether proliferated chondrocytes seeded onto a 75:25 poly(L-lactide-ε-caprolactone) sponge coated with type I collagen can be used to generate neocartilage in vivo and 2) to evaluate the relationship between the phenotype of serial passaged cells and subsequent chondrogenesis. Here we provide evidence of a correlation between cartilage regeneration and the phenotype of the serial passaged chondrocytes used to construct engineered cartilage grafts.

Materials and Methods

CONSTRUCTION OF THE BIODEGRADABLE POLYMER SCAFFOLD

The scaffold for this study was prepared with a 75:25 poly(L-lactide-ε-caprolactone) sponge coated with collagen (75-PLC scaffold). Poly(L-lactide-ε-caprolactone) scaffolds were constructed from poly(L-lactic acid) and ε-caprolactone in a ratio of 75% lactic acid to 25% ε-caprolactone. The copolymers were the generous gift of Gunze Limited (Ayabe, Japan). The scaffolds were sterilized with ethylene oxide and degassed under vacuum for 4 weeks and then coated with type I collagen (Vitrogen 100; Collagen Corp, Palo Alto, CA). The collagen-coated polymer scaffolds were washed 3 times with Hanks' balanced salt solution (HBSS) (GIBCO, Grand Island, NY) before seeding. For electron microscopy, some scaffolds were sputter-coated with gold and observed using a scanning electron microscope (JSM-5800LV; JEOL, Tokyo, Japan) (Fig 1). The average diameter of the pores in the scaffolds was 100 μm, which was consistent with the reported value.[13,14] In a previous report, we evaluated the mechanical strength of the poly(lactide-ε-caprolactone) sponge.[11] The strength of this pore size was better than that with the larger pores.[11]

CELL CULTURE

Chondrocyte cultures were established as described previously.[11] Briefly, costochondral cartilage from 4-week-old male Lewis rats was removed from adjacent fibrous tissue. The resting zone cartilage was separated and cut with surgical scissors into cross sections approximately 3 mm thick. These sections

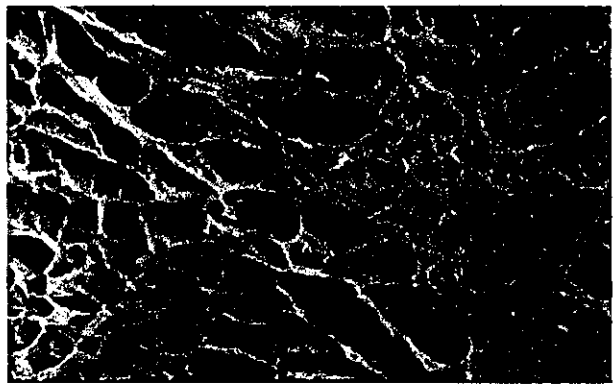

FIGURE 1. Scanning electron photomicrograph of a newly developed scaffold for chondrocytes: collagen-coated 75:25 poly(L-lactide-ε-caprolactone).

Honda et al. Cartilage Formation by Passaged Chondrocytes. J Oral Maxillofac Surg 2004.

were then immersed in phosphate-buffered saline (PBS^-) (pH 7.4) without magnesium and calcium (Takara Biomedical Pharmaceutical Co, Ltd, Otsu, Japan) containing 0.1% (w/v) EDTA twice for 20 minutes and then in PBS^- containing 0.25% (w/v) trypsin/0.05% (w/v) EDTA (GIBCO) at 37°C for 1 hour. After 3 washes with PBS^-, the tissues were digested in PBS with magnesium and calcium (PBS^+) (GIBCO) containing 0.1% (w/v) collagenase (Wako Pure Chemical Industries Ltd, Osaka, Japan) at 37°C for 4 hours. After washing with PBS^-, the digested cartilage tissues were incubated on plastic culture dishes (Falcon; Becton Dickinson & Co, Lincoln Park, NJ) in Dulbecco's modified Eagle's medium (DMEM) (GIBCO) supplemented with 10% (v/v) fetal calf serum (GIBCO) with penicillin (100 U/mL) and streptomycin (100 μg/mL) in a humidified atmosphere containing 5% (v/v) CO_2 at 37°C. The culture medium was replaced every 3 days.

When the cells reached subconfluence, the dishes were trypsinized (trypsin/EDTA; GIBCO). Thereafter, cells were cultured in a monolayer from P2 to P4. Photomicrographs were obtained from each passage of the chondrocytes using a phase-contrast electron microscope.

GROWTH OF THE CHONDROCYTES

For assessment of the kinetics of cell growth, chondrocytes were seeded onto a 6-well tissue culture dish (Falcon; Becton Dickinson & Co.) at a density of 20,000 cells/cm^2 (equivalent to ≈10% confluency). At 2, 4, 6, and 10 days, the plates were rinsed gently with HBSS (GIBCO), and at various intervals, cultures were subjected to enzymatic dissociation with trypsin and collagenase as described earlier, and the cell numbers were determined by counting an aliquot of the resulting suspension in a hemocytometer. Cellular viability was assessed with a trypan blue exclusion assay.

NORTHERN BLOT ANALYSIS

For RNA isolation, total RNA was obtained from 1-week-old rat cartilage and cultured chondrocytes using TRIZOL reagent (Life Technologies, Rockville, MD) according to the manufacturer's protocol. Reverse transcription was performed using oligo(dT) primer and SuperScript II RNase H^- reverse transcriptase (Life Technologies) according to the manufacturer's protocol. The following polymerase chain reaction (PCR) was performed in a Model 2400 GeneAmp PCR System (Perkin Elmer, Yokohama, Japan) using Amplitaq DNA polymerase (Perkin Elmer) under conditions of 30 to 40 cycles at 94°C for 1 minute, 57°C for 1 minute, 72°C for 1 minute, and finally 72°C for 10 minutes. The specific primers used for PCR were designated as type I collagen (b), type II collagen (c), and glyceraldehyde-3-phosphate dehydrogenase (GAPDH) (d), each of which was composed of a forward and a reverse primer: type I collagen, 5'-CGCGGATCCTACTGGATCGACCCTAACCAAG-3' and 5'-CGGAATTCGCACTTTTGGTTTTTGGTCACG-3'; type II collagen, 5'-CGCGGATCCTGGCTTAGGCAGAGAGAGAAG-3' and 5'-CGGAATTCTATCAGGTCAGGTCAGCCATTC-3'; and GAPDH, 5'-GCATGGCCTTCCGTGTTCCTAC-3' and 5'-GTCCACCACCCTGTTGCTGTAG-3'.

The final products were resolved and purified by electrophoresis on a 2.0% (w/v) agarose gel and used as probes for Northern blot analysis. Total RNA (20 μg) prepared from cartilage tissue or cultured chondrocytes was denatured in 50% (v/v) formamide, 5% (v/v) formaldehyde, and 20 mM 3-(N-morpholino)propanesulfonic acid, pH 7.0, at 65°C for 15 minutes and electrophoresed in 1.0% (w/v) agarose gel containing 5% (v/v) formaldehyde and then transferred to a NitroPlus membrane (Funakoshi Co Ltd, Tokyo, Japan) overnight. The transferred RNA was fixed by heating at 80°C for 2 hours and prehybridized in a solution containing 50% (v/v) formamide, 2× standard saline citrate (SSC), 1× Denhardt's solution, 0.1% (w/v) sodium dodecyl sulfate (SDS), and 0.05 mg/mL denatured salmon sperm DNA for 4 hours at 42°C. pRPC3 *EcoR*I fragment of rat aggrecan cDNA (kindly given by Dr Y. Yamada, National Institute of Dental and Craniofacial Research, Bethesda, MD) collagen types I and II, and GAPDH cDNAs were ^{32}P-labeled using a random primer labeling kit (Pharmacia Biotechnology, Uppsala, Sweden). Hybridization was carried out in the same buffer containing a ^{32}P-labeled probe for 16 hours at 42°C. The filters were washed once at 50°C in 2× SSC and 0.1% (w/v) SDS for 20 minutes, once at 50°C in 1× SSC, and 0.1% (w/v) SDS for 20 minutes, once at 50°C in 0.5× SSC and 0.1% (w/v) SDS for 20 minutes, and once at 50°C in 0.2× SSC and 0.1% (w/v) SDS for 20 minutes and then subjected to a FUJIX BAS-2000 II bioimaging analyzer (Fuji Photo Film Co, Minamiashikaga, Japan). Films were scanned, and the intensity of band hybridization to the aggrecan, collagen types I and II, and GAPDH probes was quantified by densitometry using Scion Image software (release beta 4.0.2; Scion, Frederick, Maryland) and normalized to the intensity of the GAPDH band.

PREPARATION OF CHONDROCYTE–HYBRID PLC COMPOSITES AND TRANSPLANTATION

Chondrocyte cultures reached confluence in 21 days. At preconfluence at 18 days, chondrocytes were treated with 0.25% (w/v) trypsin/0.01% (w/v) EDTA for 15 minutes. Cells dissociated from P1 to P4 cultures were collected as a suspension (1×10^7 cells/mL) in DMEM and inoculated into a 75-PLC scaffold (7 × 7 × 2 mm). The cells were injected into the scaffold using a 23-gauge syringe. Chondrocyte–75-PLC scaffold composites (CPCs) were incubated for 2 hours at 37°C under 5% (v/v) CO_2 to attach the cells to the scaffold.

Athymic KSN nude mice were anesthetized by intramuscular injection with pentobarbital sodium. The dorsal side was scrubbed with antiseptic solution. A 1-cm-long cross incision was made between the scapulae. A subcutaneous pocket was prepared by blunt dissection on the front sides of the midline incision. The CPCs were placed into the pocket, and the wound was closed in layers with 4.0 Vicryl interrupted sutures. Ten rats were prepared for grafting for each series of passaged cells.

HISTOLOGY

At 4 weeks after the implantation the mice were killed, and each CPC was dissected along with the surrounding fibrous tissue capsule. Thereafter, CPCs were fixed in 10% buffered formalin for 24 hours, dehydrated with graded ethanol, and embedded in paraffin. Then, 5-μm-thick paraffin sections were deparaffinized with xylene, rehydrated, and stained with hematoxylin-eosin or Alcian blue (pH 1.0) to detect the presence of sulfated glycosaminoglycans.

Results

PROPERTIES OF 75-PLC SCAFFOLD

A scanning electron photomicrograph of the scaffold showed a nonfiber sponge structure with numerous pores (Fig 1). A smooth-textured surface and regular porous structure were achieved for the polymer scaffold. The scaffolds had a nominal pore size averaging 100 μm (SD, ±50 μm) in diameter.

PHASE-CONTRAST MORPHOLOGY

Figure 2 illustrates the phase-contrast morphology of rat costal chondrocytes cultured in plastic dishes.

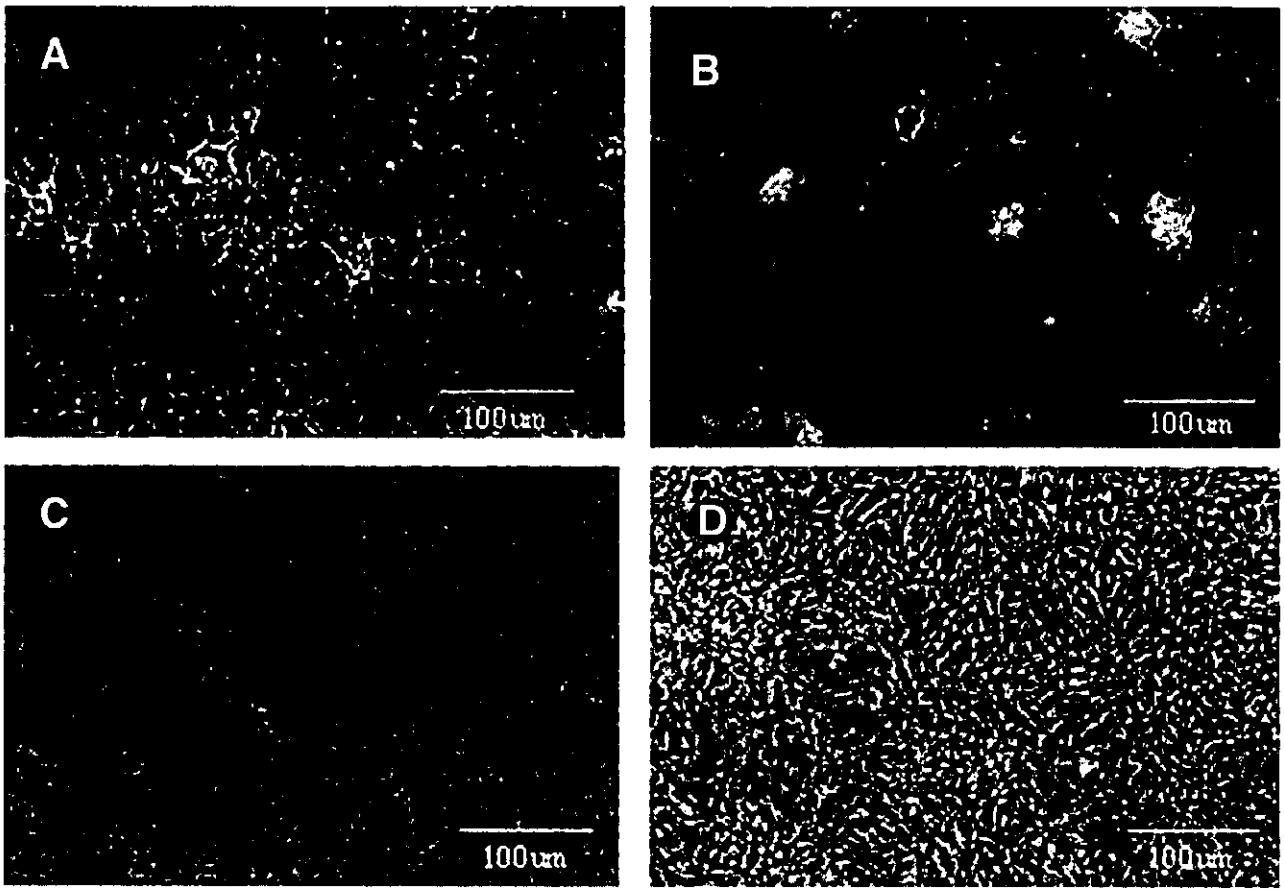

FIGURE 2. Phase-contrast morphology of the serial passaged culture cells: *A*, first passage of chondrocytes; *B*, second passage of chondrocytes; *C*, third passage of chondrocytes; *D*, fourth passage of chondrocytes.

Honda et al. Cartilage Formation by Passaged Chondrocytes. J Oral Maxillofac Surg 2004.

P1 chondrocytes reached confluence on day 12 and retained the polygonal shape characteristic of cultured chondrocytes[4,10,15] (Fig 2A). The shape of the P2 chondrocytes was similar to that observed in P1 chondrocytes, which had a polygonal shape (Fig 2B). However, when chondrocytes were grown on the tissue culture dish from P3 to P4, the cells became elongated with small processes, assuming a fibroblast-like appearance (Figs 2C, D). The hypertrophic chondrocytes showed a significant difference as found in P3 and P4 chondrocytes.

GROWTH OF CHONDROCYTES

The number of cells in the cultures at various intervals after plating were determined as an index of chondrocyte proliferation (Fig 3). The viability of the cells was greater than 95% at all times examined. The growth of P1 chondrocytes was slower than that of P4 chondrocytes and the growth rate increased with passages. However, there were no significant differences.

NORTHERN BLOT ANALYSIS

Northern blot analysis of RNA extracted from serial passaged cultures of chondrocytes revealed a distinct pattern of expression of aggrecan and collagen types I and II messenger RNA (mRNA) (Fig 4A), normalized to GAPDH mRNA. These results are illustrated in Figure 4B. With the progress of each passage, the expression of the aggrecan and collagen type II mRNA gradually decreased (aggrecan: P1 53%, P2 38%, P3 25%, P4 13%; type II collagen: P1 55%, P2 54%, P3 42%, P4 17%), whereas collagen type I mRNA was weakly detectable on primary culture and then increased during the following passages (collagen type I: P1 27%, P2 58%, P3 69%, P4 76%).

CARTILAGE FORMATION IN VIVO IN SCAFFOLD

A gross morphologic assessment 4 weeks after implantation showed that the implanted composites formed a solid whitish-yellow tissue. The CPCs maintained the original shape of the 75-PLC scaffold before implantation. Figure 5 shows that cartilage formation was more prominent in the P1 and P2 chondrocyte

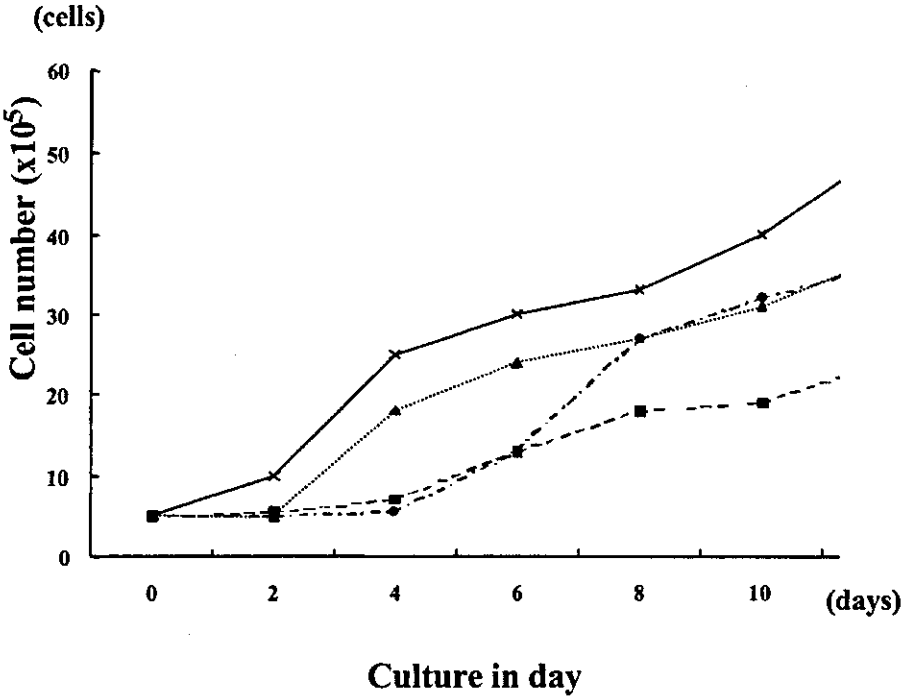

FIGURE 3. Growth of the serial passaged cells in the new scaffolds: black circle, first passage of chondrocytes; black square, second passage of chondrocytes; black triangle, third passage of chondrocytes; cross, fourth passage of chondrocytes.

Honda et al. Cartilage Formation by Passaged Chondrocytes. J Oral Maxillofac Surg 2004.

groups. With regard to P2 chondrocytes, the proportion of cartilage-like tissue in the scaffold was approximately 80% of that observed with P1 chondrocyte CPSs. Fibrous tissue containing vascular elements was also observed. The extracellular matrix around the cells was stained with Alcian blue (Fig 5A), suggesting an abundant accumulation of sulfated glycosaminoglycans in the extracellular matrix surrounding the inoculated chondrocytes. However, in the composites with P3 chondrocytes, cartilage-like tissue was also observed in half of the 10 specimens (Table 1), although the proportion of such tissue in the specimens was only 10% to 20% of that of P1 CPCs (Fig 5B). P4 chondrocytes did not show cartilage-like tissue formation, and fibrous connective tissue was observed in the specimens (Fig 5C). Vascular ingrowth was found to be present in all implants. Thus, the number of cell passages used to establish chondrocyte cultures influenced the percentage of Alcian blue–positive staining in CPCs. In the absence of cultured chondrocytes, the implantation of polymer scaffolds alone did not result in neocartilage formation.

Discussion

Tissue engineering is one of the most promising approaches to cartilage repair. However, should this

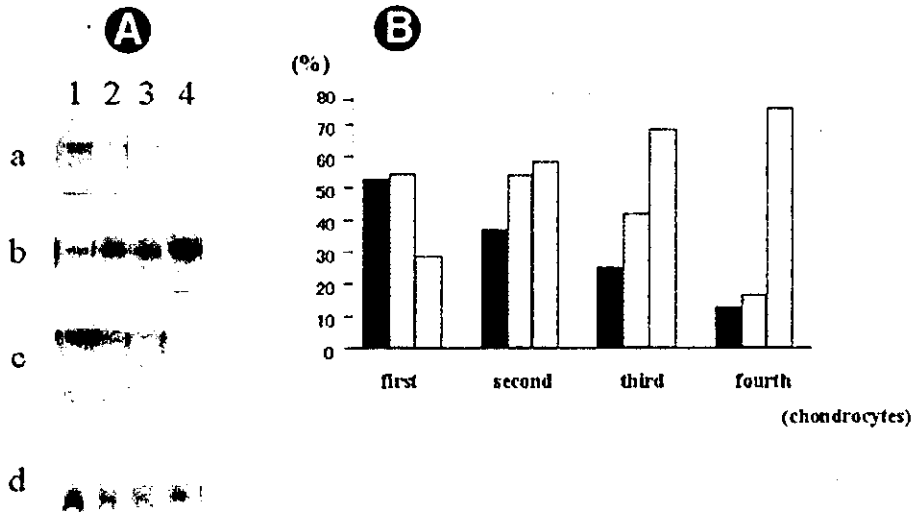

FIGURE 4. (A) Aggrecan and types I and II collagen gene expression of the serial passaged chondrocytes on static dish using Northern blot analysis: a, aggrecan; b, type I collagen; c, type II collagen. The blot was hybridized with a GAPDH probe as an internal control (d): lane 1, first passage of chondrocytes; lane 2, second passage of chondrocytes; lane 3, third passage of chondrocytes; lane 4, fourth passage of chondrocytes. (B) Densitometric analysis of Northern blot findings hybridized with aggrecan and types I and II collagen normalized with respect to the corresponding GAPDH signal. Black box, aggrecan; gray box, type II collagen; white box, type I collagen.

Honda et al. Cartilage Formation by Passaged Chondrocytes. J Oral Maxillofac Surg 2004.

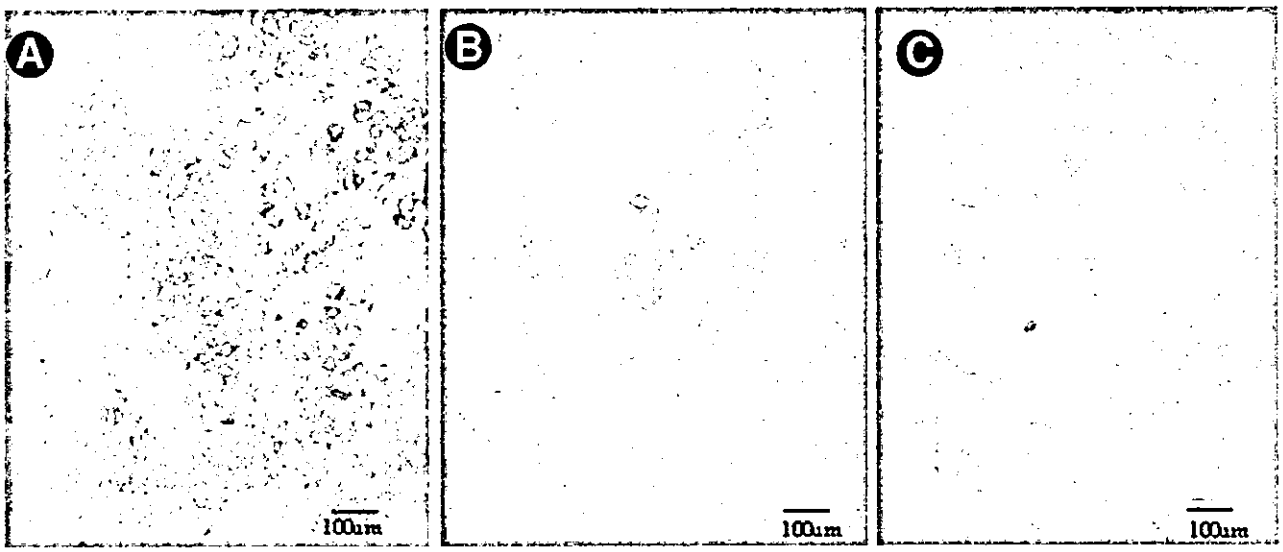

FIGURE 5. Histologic picture of cartilage formation in vivo stained with Alcian blue: *A*, 4 weeks after second passage of chondrocyte implantation; *B*, 4 weeks after third passage of chondrocyte implantation; *C*, 4 weeks after fourth passage of chondrocyte implantation.

Honda et al. Cartilage Formation by Passaged Chondrocytes. J Oral Maxillofac Surg 2004.

method be applied to the maxillofacial region, an abundant supply of chondrocytes would likely be required, particularly when the graft is for reconstruction of the ear, nose, trachea, or temporomandibular joints. Saadeh et al[16] reported that the chondrocyte density required for optimum cartilage formation in a construct is 25 to 50 $\times$ 10^6 cells/mL. The typical volume needed for a clinically significant construct, such as an ear, would be approximately 5 mL, requiring 1.25 to 2.50 $\times$ 10^7 cells.[16] Our strategy is to develop a method for generating a large quantity of well-differentiated chondrocytes in vitro, thus providing sufficient cells to implant and seed in a suitably shaped biodegradable scaffold. At the present, monolayer culture is the most efficient method for obtaining such a large number of cells. However, it is well known that cultures of chondrocytes tend to lose their phenotype over time.[8-10] In this study, we evaluated whether serial passaged chondrocytes in monolayer cultures could be used to regenerate cartilage-like tissue when the cells were seeded in a 75-PLC scaffold. We show that the scaffold is capable of supporting chondrogenesis when seeded with early-passage cells (P1 or P2) but not late-passage cells (P4).

The gross morphology of P4 chondrocytes on phase contrast was similar to that of the fibroblastic cells and was distinct from the hypertrophic appearance of P1 to P3 chondrocytes. This observation suggests that hypertrophic cells play a role in cartilage formation. This distinct difference may provide a useful way of judging cellular function on the basis of chondrogenesis.

The phenotype of differentiated chondrocytes is marked by the predominant synthesis of aggrecan, whereas the dedifferentiated fibroblast-like phenotype is marked by collagen type I.[17-19] Aggrecan and collagen types I and II mRNAs were detected in P1 to P4 chondrocytes using Northern blot analysis. Aggre-

Table 1. HISTOLOGIC EVIDENCE OF CARTILAGE TISSUE FORMATION IN COMPOSITE

Cartilage Tissue Staining Positive (%)	P1 Chondrocyte	P2 Chondrocyte	P3 Chondrocyte	P4 Chondrocyte
>90				
75 to 90	5			
50 to 75	5	2		
25 to 50		7	4	
25<		1	6	
0				10

NOTES. Cells were cultured in monolayers until P1 and P4 (passages 1 and 4). The composite were transplanted into the subcutaneous dorsum of nude mice. Four weeks after transplantation, the composites were fixed and analyzed using Alcian blue staining. The mean percent is the proportion of the new cartilage tissue formation inside the grafted scaffold.

Honda et al. Cartilage Formation by Passaged Chondrocytes. J Oral Maxillofac Surg 2004.

can and collagen type II mRNA decreases further with each cell passage, whereas collagen type I mRNA increased with each passage of cells. Cartilage formation ceased to occur when the expression levels of aggrecan mRNA and collagen type II mRNA decreased to about 30% and 80% of those of P1 chondrocytes, respectively.

In summary, using tissue-engineering methods, we evaluated the correlation between cartilage formation and proliferated chondrocytes. Northern blot analysis is useful in determining whether chondrocytes are capable of regenerating cartilage tissue. This study should encourage further studies on improving the scaffold to maintain the phenotype of chondrocytes.

Acknowledgments

The authors are very appreciative of the help of Dr N. Morikawa (Gunze Limited) in preparing the polymer scaffolds. They are also grateful to Dr Y. Ikada (Kyoto University) for several stimulating discussions.

References

1. Schaefer D, Martin I, Jundt G, et al: Tissue-engineered composites for the repair of large osteochondral defects. Arthritis Rheum 46:2524, 2002
2. Freed LE, Martin I, Vunjak-Novakovic G: Frontiers in tissue engineering. In vitro modulation of chondrogenesis. Clin Orthop S46:367, 1999 (suppl)
3. Cao Y, Vacanti JP, Paige KT, et al: Transplantation of chondrocytes utilizing a polymer-cell construct to produce tissue-engineered cartilage in the shape of a human ear. Plast Reconstr Surg 100:297, 1997
4. Vacanti CA, Langer R, Schloo B, et al: Synthetic polymers seeded with chondrocytes provide a template for new cartilage formation. Plast Reconstr Surg 88:753, 1991
5. Sherwood JK, Riley SL, Palazzolo R, et al: A three-dimensional osteochondral composite scaffold for articular cartilage repair. Biomaterials 23:4739, 2002
6. van Osch GJ, Marijnissen WJ, van der Veen SW, et al: The potency of culture-expanded nasal septum chondrocytes for tissue engineering of cartilage. Am J Rhinol 15:187, 2001
7. de Haart M, Marijnissen WJ, van Osch GJ, et al: Optimization of chondrocyte expansion in culture. Effect of TGF beta-2, bFGF and L-ascorbic acid on bovine articular chondrocytes. Acta Orthop Scand 70:55, 1999
8. Benya PD, Paddila SR, Nimni ME: Independent regulation of collagen types of chondrocytes during the loss of differentiated function in culture. Cell 15:1313, 1978
9. Takigawa M, Shirai E, Fukuo K, et al: Chondrocytes dedifferentiated by serial monolayer culture form cartilage nodules in nude mice. Bone Miner 2:449, 1987
10. Benya PD, Shaffer JD: Dedifferentiated chondrocytes reexpress the differentiated collagen phenotype when cultured in agarose gels. Cell 30:373, 1982
11. Honda M, Yada T, Ueda M, et al: Cartilage formation by cultured chondrocytes in a new scaffold made of poly(L-lactide-ε-caprolactone) sponge. J Oral Maxillofac Surg 58:767, 2000
12. Honda M, Morikawa N, Hata K, et al: Rat costochondral cell characteristics on poly (L-lactide-co-epsilon-caprolactone) scaffold. Biomaterials 24:3511, 2003
13. Suzuki S, Matsuda K, Issiki N, et al: An artificial skin composed of an outer layer of silicone and an inner layer of collagen and GAG. Jpn J Plast Reconstr Surg 31:298, 1988
14. Yannas IV, Lee E, Orgill DP, et al: Synthesis and characterization of a model extracellular matrix that induced partial regeneration of adult mammalian skin. Proc Natl Acad Sci U S A 86:933, 1989
15. van Osch GJ, van der Veen SW, Verwoerd-Verhoef H: In vitro redifferentiation of culture-expanded rabbit and human auricular chondrocytes for cartilage reconstruction. Plast Reconstr Surg 107:433, 2001
16. Saadeh PB, Brent B, Mehrara BJ, et al: Human cartilage engineering chondrocyte extraction, proliferation, and characterization for construct development. Ann Plast Surg 42:509, 1999
17. Ronziere MC, Roche S, Gouttenoire J, et al: Ascorbate modulation of bovine chondrocyte growth, matrix protein gene expression and synthesis in three-dimensional collagen sponges. Biomaterials 24:851, 2003
18. Homicz MR, Schumacher BL, Sah RL, et al: Effects of serial expansion of septal chondrocytes on tissue-engineered neocartilage composition. Otolaryngol Head Neck Surg 127:398, 2002
19. Matyas JR, Huang D, Chung M, et al: Regional quantification of cartilage type II collagen and aggrecan messenger RNA in joints with early experimental osteoarthritis. Arthritis Rheum 46: 1536, 2002

THE JOURNAL OF BIOLOGICAL CHEMISTRY
Vol. 279, No. 32, Issue of August 6, pp. 33281–33289, 2004
Printed in U.S.A.

A Novel Mechanism for the Inhibition of Hyaluronan Biosynthesis by 4-Methylumbelliferone*

Received for publication, May 27, 2004
Published, JBC Papers in Press, June 9, 2004, DOI 10.1074/jbc.M405918200

Ikuko Kakizaki‡, Kaoru Kojima‡, Keiichi Takagaki‡, Masahiko Endo‡, Reiji Kannagi§¶, Masaki Ito‖, Yoshihiro Maruo, Hiroshi Sato‡‡, Tadashi Yasuda§§, Satoka Mita§§¶¶, Koji Kimata§§, and Naoki Itano‡§§‖‖**

*From the ‡Department of Biochemistry, Hirosaki University School of Medicine, 5 Zaifu-cho, Hirosaki 036-8562, §Program of Molecular Pathology, Aichi Cancer Center, Research Institute, Nagoya 464-8681, ¶Core Research for Evolutional Science and Technology, Japan Science and Technology Agency, ‖Second Department of Internal Medicine, the **Department of Pediatrics and the ‡‡Department of Biology, Shiga University of Medical Science, Seta, Otsu, Shiga, the ¶¶Department of Biochemistry, Osaka University Medical School, 2-2 Yamadaoka, Suita, Osaka 565-0871, and §§Institute for Molecular Science of Medicine, Aichi Medical University, Nagakute, Aichi 480-1195, Japan*

Specific inhibitors of hyaluronan (HA) biosynthesis can be valuable therapeutic agents to prevent cancer invasion and metastasis. We have found previously that 4-methylumbelliferone (MU) inhibits HA synthesis in human skin fibroblasts and in group C *Streptococcus*. In this paper, the inhibition mechanism in mammalian cells was investigated using rat 3Y1 fibroblasts stably expressing HA synthase (HAS) 2. Exposure of the transfectants to the inhibitor resulted in significant reduction of HA biosynthesis and matrix formation. The evaluation of HAS transcripts and analysis of cell-free HA synthesis demonstrated the post-transcriptional suppression of HAS activity by MU. Most interesting, the post-transcriptional suppression of HAS activity was also observed using *p*-nitrophenol, a well known substrate for UDP-glucuronyltransferases (UGT). We investigated whether the inhibition was exerted by the glucuronidation of MU using both high pressure liquid chromatography and TLC analyses. The production of MU-glucuronic acid (GlcUA) was consistent with the inhibition of HA synthesis in HAS transfectants. MU-GlcUA was also detected at a similar level in control cells, suggesting that the glucuronidation was mediated by an endogenous UGT. Elevated levels of UGT significantly enhanced the inhibitory effects of MU. In contrast, the inhibition by MU was diminished to the control level when an excess of UDP-GlcUA was added to the cell-free HA synthesis system. We propose a novel mechanism for the MU-mediated inhibition of HA synthesis involving the glucuronidation of MU by endogenous UGT resulting in a depletion of UDP-GlcUA.

There are a considerable number of reports showing that the biosynthesis of hyaluronan (HA)[1] is elevated in disorders such as fibroses of organs, diseases associated with inflammation, and some types of tumors including mesothelioma and Wilm's tumor (1–5). For instance, accumulation of HA is associated with the progression of atherosclerosis (6). During the progression of hepatitis, HA derived from the Ito cells accumulates in the liver, causing fibrosis and eventually cirrhosis of the liver (7). Because HA is directly associated with liver fibrosis, it has long been utilized as a marker for the diagnosis of chronic hepatitis (8). Also, an exponential increase of HA in the endocervical canal at inappropriate stage of pregnancy can result in miscarriage (9). Recent genetic approaches showed that overproduction of HA accelerated tumor growth and is associated with cancer metastasis (10–14).

HA is a nonsulfated linear glycosaminoglycan composed of thousands of repeating units of GlcNAc-β(1→4)-GlcUA-β(1→3) (15). In vertebrates, this molecule is a ubiquitous component of the extracellular matrix and plays critical roles in dynamic functions such as embryonic development, tissue regeneration, and cell migration (16). Both eukaryotic and prokaryotic HA synthases (HAS) catalyze the transglycosylation from both UDP-GlcUA and UDP-GlcNAc donors (17). Following the first cloning of a HAS gene from *Streptococcus* in 1993, three distinct mammalian isoforms, HAS1, HAS2, and HAS3, have been identified and characterized from mouse, human, and other species (17). Considerable progress in understanding HA biosynthesis and its biological functions has been made in recent years.

Identification of a specific inhibitor for HA biosynthesis would not only help elucidate the functions of HA but would also have applications in clinical medicine for the treatment of diseases caused by elevated levels of this glycosaminoglycan. Over the past few decades many researchers have attempted without success to discover specific inhibitors of HA synthesis in mammalian cells (18–22). 4-Methylumbelliferone (MU, 7-hydroxy-4-methyl-2*H*-1-benzopyran-2-one) was found previously to inhibit HA synthesis in cultured human skin fibroblasts but had no effect on the synthesis of any other glycosaminoglycan (23, 24). Since then MU has been used as an

* This work was supported by grants from the CREST of Japan Science and Technology Agency, a preparatory grant for research at the Division of Matrix Glycoconjugates, Research Center for Infectious Disease, Aichi Medical University, grants-in-aid for young scientists (B), Grants-in-aid for Scientific Research on Priority Areas from the Japan's Ministry of Education, Culture, Sports, Science, and Technology 14780480 and 15040203, Grant-in-aid for Scientific Research (B) from Japan Society for the Promotion of Science 15370041, the Aichi Cancer Research Foundation, grant-in-aid from the Tokyo Biochemical Research Foundation, special research funds from Seikagaku Corp., and the Karoji Memorial Fund for Medical Research (A) and (B) in Hirosaki University. The costs of publication of this article were defrayed in part by the payment of page charges. This article must therefore be hereby marked "*advertisement*" in accordance with 18 U.S.C. Section 1734 solely to indicate this fact.

‖‖ To whom correspondence should be addressed. Tel.: 81-52-264-4811 (ext. 2095); Fax: 81-561-63-3532; E-mail: itano@amugw.aichi-med-u.ac.jp.

[1] The abbreviations used are: HA, hyaluronan; MU, 4-methylumbelliferone; *p*NP, *p*-nitrophenol; GlcUA, glucuronic acid; GlcNAc, *N*-acetylglucosamine; Glc, glucose; HA synthase, HAS; Me_2SO, dimethyl sulfoxide; PBS, phosphate buffered saline; DTT, dithiothreitol; UGT, UDP-glucuronosyltransferase; HPLC, high pressure liquid chromatography; ELISA, enzyme-linked immunosorbent assay; RT, reverse transcriptase.

inhibitor of HA synthesis in many studies on the functions of HA, although its precise mechanism has not been established in mammalian cells (10, 25, 26).

For many years MU has been used safely in human medicine as a cholagogue by oral administration (27). The clinical application of MU for controlling HA synthesis could potentially prevent malignant alteration of cancer cells and fibrosis of organs. It would therefore be helpful to clarify the inhibition mechanism of MU in mammalian cells. The information may also be useful in developing new compounds that are more effective inhibitors and/or display lower cytotoxicity than MU. A possible phospholipid-dependent inhibition mechanism of MU was found using group C *Streptococcus* in our previous paper (28). We suggested that MU treatment may inhibit HAS activity by altering the distribution of cardiolipin species surrounding HAS in the plasma membrane. However, the change in the distribution of cardiolipin cannot by itself account for the observed inhibition of HA synthesis. Furthermore, the proposed mechanism of inhibition involving cardiolipin might be specific for *Streptococcus*, because mammalian cells have low levels of cardiolipin in the plasma membrane. Indeed the effect of cardiolipin on enzymatic activity is distinct between mammalian HAS1 and streptococcal HAS (29), suggesting that the MU-mediated inhibition is quite complex. In this study we demonstrate a UGT-dependent inhibition mechanism for HA synthesis in mammalian cells using transfectants that express mouse HAS2. We propose the inhibition of HA synthesis is due, in part, to a depletion in the pool of UDP-GlcUA, a common substrate of HAS and UGT.

EXPERIMENTAL PROCEDURES

Materials and Reagents—MU was purchased from Wako Pure Chemicals (Osaka, Japan). *p*-Nitrophenol (*p*NP), *p*NP-sugars (*p*NP-Glc, *p*NP-GlcUA, and *p*NP-GlcNAc), and MU-sugars (MU-Glc, MU-GlcUA, and MU-GlcNAc) were from Sigma. MU and MU-sugars were dissolved in dimethyl sulfoxide (Me_2SO); *p*NP and *p*NP-sugars were dissolved in ethanol, and the final concentration of these vehicles in the culture medium and the reaction mixtures for the cell-free HA synthesis were adjusted to 0.1%. UDP-[^{14}C]GlcUA (313 mCi/mmol) and [^{14}C]*p*NP (70 mCi/mmol) were from ICN Biomedicals, Inc. (Irvine, CA) and American Radiolabeled Chemicals Inc. (St. Louis, MO), respectively. UDP-GlcUA, dithiothreitol (DTT), and ATP were from Nakalai Tesque (Kyoto, Japan). UDP-GlcNAc, bovine liver β-glucuronidase, and glutaraldehyde-stabilized sheep erythrocytes were from Sigma. *Streptomyces* hyaluronidase was obtained from Seikagaku Corp. (Tokyo, Japan). Hyaluronic acid "Chugai" quantitative test kit for the sandwich binding protein assay was purchased from Chugai Pharmaceutical (Tokyo, Japan) (30). Recombinant human UGT1A6 and UGT1A7 proteins were from Calbiochem, and their expression vectors were reported previously (31).

Cell Culture and Transfection—Stable transfectants were established by transfection of mouse HAS2 and control vector into rat 3Y1 cells as described previously (32). Cells were routinely cultured in Dulbecco's modified Eagle's medium containing 10% fetal calf serum, 2 mM L-glutamine, and 400 μg/ml G418 at 37 °C. pFLAG-HAS2 and human UGT1A6 expression vector were transiently transfected into COS-1 cells by electroporation as described previously (32). The cells were cultured in Dulbecco's modified Eagle's medium containing 10% fetal calf serum and 2 mM L-glutamine at 37 °C.

Particle Exclusion Assay—3Y1-HAS2 cells plated at 1×10^3 cells in a 35-mm dish were cultured for 2 days and then further cultured for a day with or without 300 μM MU. An aliquot of glutaraldehyde-stabilized sheep erythrocytes (3×10^8) in PBS was then added to the culture medium. After 15 min, the culture was observed using an inverted phase-contrast microscope (Olympus IMT-2) (33).

Quantitative Analyses of the HAS Transcripts—The relative level of HAS expression in the HAS2 transfectants was determined by real time quantitative RT-PCR as described previously (11). The gene-specific PCR primers and probes were designed from the mouse HAS2 and rat HAS sequences using the Primer Express software (Applied Biosystems, Foster City, CA). The sequences of the various oligonucleotides are as follows: the forward primer for mouse HAS2 was 5′-CCTCGGAATCACAGCTGCTTATA-3′, and the reverse primer was 5′-CTGCCCATAACTTCGCTGAATA-3′; the probe for mouse HAS2 was 5′-TCGCATCTCATCATCCAAAGCCTCTTTG-3′; the forward primer for rat HAS1 was 5′-GGAGATGTGAGAATCCTTAACCCTC-3′, and the reverse primer was 5′-TGCTGGCTCAGCCAACGAAGGAA-3′; the probe for rat HAS1 was 5′-CAGAGCTACTTTCACTGTGTGTCCTGCATC-3′; the forward primer for rat HAS2 was 5′-CCTCGGAATCACAGCTGCTTATA-3′, and the reverse primer was 5′-CTGCCCATGACTTCACTGAAGA-3′; the probe for rat HAS2 was 5′-TCACACCTCATCATCCAAAGCCTCTTTG-3′; the forward primer for rat HAS3 was 5′-GGTACCATCAGAAGTTCCTAGGCAGC-3′, and the reverse primer was 5′-GAGGAGAATGTTCCAGATGCG-3′; and the probe for rat HAS3 was 5′-TGGCTACCGGACTAAGTATACAGCACGCTC-3′. Total RNA was isolated from subconfluent rat 3Y1 cells expressing mouse HAS2 using the RNeasy mini kit (Qiagen, Valencia, CA). Two hundred nanograms of total RNA was used for real time RT-PCR and subsequent analysis. The reaction master mix was prepared to give final concentrations of 1× TaqMan EZ buffer, 0.3 mM dATP, 0.3 mM dCTP, 0.3 mM dGTP, 0.6 mM dUTP, 6 mM manganese acetate, 0.01 units/μl uracil *N*-glycosylase, 0.1 units/μl rTth DNA polymerase, 200 nM primers, and 100 nM TaqMan probe. The conditions for RT-PCR are as follows: 1 cycle at 50 °C for 2 min, 1 cycle at 60 °C for 30 min, 1 cycle at 95 °C for 5 min, 50 cycles at 95 °C for 20 s, and 60 °C for 1 min. Fluorescent signals generated during PCR amplifications were monitored in real time using the 7700 sequence detector system (Applied Biosystems) and analyzed with the sequence detector 1.7 program (Applied Biosystems). The relative amount of glyceraldehyde-3-phosphate dehydrogenase mRNA was measured using the TaqMan rodent glyceraldehyde-3-phosphate dehydrogenase detection reagents (Applied Biosystems). The amount of HAS mRNA was divided by the amount of glyceraldehyde-3-phosphate dehydrogenase mRNA in each sample. The normalized values were designated as the "relative expression coefficient" in this study. Standard curves were generated by serial dilution of total RNA isolated from HAS2 transfectants.

Determination of the HA Concentration by ELISA-like Assay—Cells were plated at a density of 1×10^5 and 8×10^5 cells/well in a 6-well plate (defined as exponentially growing phase and confluent phase, respectively). The cells were cultured with various concentrations of MU for 24 h. HA released into the culture medium was quantified by an ELISA-like assay using HA-binding protein according to the manufacturer's instructions for the hyaluronic acid "Chugai" quantitative test kit (30). The quantity of HA was expressed per live cell number. The viability of cells was assessed by trypan blue staining.

HA Synthase Assay—HAS activity was monitored in the cell-free HA synthesis system using UDP-[^{14}C]GlcUA and UDP-GlcNAc as donors and a membrane-rich fraction of the transfectants as an enzyme source as described previously (32). Briefly, the HAS transfectants were washed, harvested, and disrupted by sonication in 10 mM Hepes-NaOH, pH 7.1, 0.5 mM dithiothreitol containing 0.25 M sucrose. Suspensions of the disrupted cells were ultracentrifuged in a Beckman TLS rotor at 43,000 rpm for 1 h to give the high speed pellet. The crude membrane fractions prepared from HAS transfectants were resuspended with standard reaction mixture (0.1 ml of 25 mM Hepes-NaOH, pH 7.1, 5 mM DTT, 15 mM $MgCl_2$, 0.1 mM UDP-GlcNAc, 2 μM UDP-GlcUA, and 0.2 μCi of UDP-[^{14}C]GlcUA) and incubated at 37 °C for 1 h. Depending on the type of experiment, MU, *p*NP, and their sugar derivatives were added to the reaction mixture. Alternatively, the membrane fractions were preincubated at 37 °C for 1 h with 300 μM MU or 300 μM MU-GlcUA in the preincubation mixture (0.1 ml of 25 mM Hepes-NaOH, pH 7.1, 5 mM DTT, 15 mM $MgCl_2$, 0.1 mM UDP-GlcUA), and then HA synthesis was initiated by adding 2 mM UDP-GlcNAc and 0.2 μCi of UDP-[^{14}C]GlcUA. The reaction was terminated at the indicated time by addition of SDS to 2% (w/v). The mixtures were then spotted onto Whatman No. 3MM paper, and the paper was developed in 1 M ammonium acetate (pH 5.5) and ethanol (65:35 v/v) for 3 days. The origin, containing the synthesized polymers, was removed, and the amount of radioactivity in the high molecular mass HA was determined by liquid scintillation counting.

Agarose Gel Electrophoresis of HA—The size distribution of radiolabeled HA synthesized in the cell-free reaction was analyzed by agarose gel electrophoresis (0.5% gel) as described previously (32). The synthesized HA was incubated at 37 °C for 1 h with or without 1 turbidity reducing unit of *Streptomyces* hyaluronidase prior to loading on the gel. After drying the gel, the radioactive HA was detected using a BAS 5000 Bio-Imaging Analyzer (Fuji Film Co., Tokyo, Japan).

HPLC Analysis of the MU-sugar Derivative—MU-sugar derivatives, from culture conditioned medium and from cell lysate, were analyzed by HPLC using a TSK gel ODS-120T (15 cm × 4.6 mm inner diameter) column. HPLC conditions were identical to those described by

Zimmerman *et al.* (34). Eluted fractions were monitored by detecting fluorescence (excitation 325 nm, emission 380 nm) using a fluorescence spectrophotometer Hitachi F-1050 (Tokyo, Japan). Cells were washed with PBS three times and then disrupted in a solution of 2% SDS-PBS by sonication for 2 min (4 bursts of 30 s) using a sonifier (model UR-20P, Tomy Seiko, Tokyo, Japan). The cell lysate was then obtained by centrifugation at 105,000 × *g* for 30 min. The supernatants were used for HPLC analysis. For TLC analysis in Fig. 3 and for mass spectrometry, a peak corresponding to MU-GlcUA was collected by HPLC as described below. A fraction containing MU-GlcUA was prefractionated from culture supernatant using a Sep-Pac Plus C18 cartridge (Waters, MA) prior to HPLC. Briefly, the culture supernatant was loaded onto the cartridge, and the cartridge was then washed with water. Bound materials containing MU-GlcUA were eluted with 100% methanol, concentrated by using a vacuum evaporator centrifuge (Iwaki, Tokyo, Japan), and analyzed by HPLC. A peak of MU-GlcUA was collected and desalted using a Sep-Pac Plus C18 cartridge. After drying, the residue was dissolved into methanol and analyzed by TLC or mass spectrometry.

TLC Analysis of the MU-sugar or pNP-sugar Derivative—Radiolabeled MU-sugar or *p*NP-sugar derivatives produced in the cell-free HA synthesis system was treated with or without 2 units of β-glucuronidase at 37 °C for 1 h and then separated by TLC. TLC was performed on a Silica 60 TLC plate (Merck) using 1-butanol/ethanol/water (5:3:2, v/v/v) as the mobile phase (35). After drying the plate, radioactive spots were detected using a BAS 5000 Bio-Imaging Analyzer. The radiolabeled product derived from the incubation of *p*NP and UDP-[^{14}C]GlcUA according to the standard assay method of UGT (36) was used for determining the mobility of *p*NP-GlcUA. Fluorescent spots containing MU or MU-sugar were detected by ultraviolet irradiation using a transilluminator. Authentic MU-GlcUA was used as a standard.

Mass Spectrum Measurements—Mass spectra were obtained on a PE-Sciex API-100 single-quadrupole mass spectrometer (Thornhill, Ontario, Canada) equipped with an atmospheric pressure ionization source described previously (37). The mass spectrometer was operated in the negative mode. Samples dissolved in 50% 2-propanol were ionized by electrospray ionization and continuously infused into the electrospray ionization chamber at a flow rate of 5 μl min^{-1}.

RESULTS

Inhibitory Effect of MU on HA Production and HA Matrix Formation of the HAS2-expressing Cells—MU was originally found to inhibit HA synthesis and HA matrix formation of cultured human skin fibroblasts (23, 24). The recent discovery that MU inhibits HA synthesis of group C *Streptococcus* in a phospholipid-dependent fashion provided new insight into understanding the mechanism of inhibition (28). However, the inhibition of HA synthesis by MU cannot be explained by this mechanism alone, particularly in mammalian cells. In this study, we examined the effects of MU on HA synthesis by using HAS2 overexpressing cells in order to clarify which step of HA synthesis is the target for the inhibition. The HAS2 overexpressing cells, named 3Y1-HAS2, were established from rat 3Y1 fibroblasts by transfection with HAS2 cDNA as described previously (32). Formation of pericellular HA matrices and HA production were significantly inhibited in 3Y1-HAS2 cells by treatment with MU as observed previously in cultured human skin fibroblasts (23, 24) (Fig. 1). The formation of pericellular HA matrices was inhibited by ~30% during exposure to 300 μM MU compared with the nontreated control. The level of inhibition was even more apparent at higher concentrations of MU (data not shown). HA accumulation in the conditioned medium was dose-dependently decreased by MU treatment both in the exponentially growing and confluent phases of 3Y1-HAS2 cells (Fig. 1*E*).

Transcription of the mouse HAS2 transgene and the endogenous HAS genes in the transfectants was assessed by real time RT-PCR using mouse- and rat-specific HAS primers and probes. No obvious change in the transcriptional levels of these HAS genes was observed at the low or moderate concentrations of MU, whereas the level of the endogenous HAS2 gene was inhibited during exposure to a high dose of MU (Table I). These results suggest that MU inhibits HAS activity post-transcriptionally at the low or moderate concentrations of MU. In contrast, a high dose of MU inhibits HA synthesis by suppressing HAS functions both transcriptionally and post-transcriptionally.

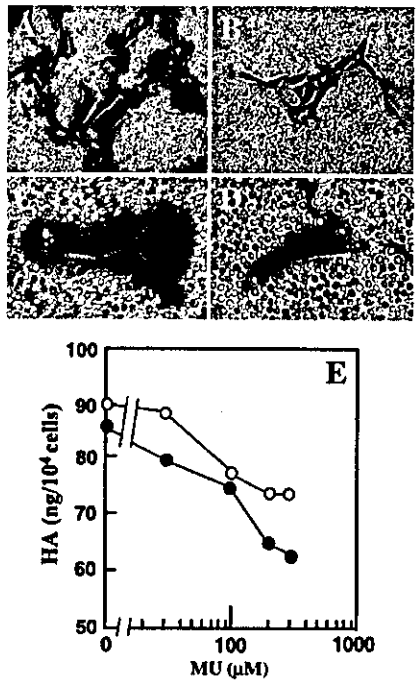

FIG. 1. **HA production and matrix formation of HAS2 transfectants after MU treatment.** *A–D*, pericellular HA matrices surrounding 3Y1-HAS2 transfectants were visualized by the particle exclusion assay, and photomicrographs were taken under inverted phase contrast microscope at ×300 (*A* and *B*) and then magnified further (*C* and *D*). The 3Y1-HAS2 cells were cultured for 24 h with (*B* and *D*) or without (*A* and *C*) 300 μM MU. *E*, the HA contents in the conditioned medium from exponentially growing (*open circles*) and confluent cultures (*closed circles*) were measured by ELISA-like assay at 24 h after the treatment of 3Y1-HAS2 transfectants with various concentrations of MU. Data represent average of two independent experiments.

TABLE I
Relative HAS expression in HAS2 transfectants after MU treatment

MU	Mouse HAS2	Rat HAS2	Rat HAS3
μM	%	%	%
0	100	100	100
10	130.7 ± 19.7	94.7 ± 25	98.5 ± 13.9
30	129.1 ± 34.8	86.1 ± 10.7	93.1 ± 13.7
100	137.4 ± 11.6	105.0 ± 28	93.9 ± 10.3
300	93.3 ± 29.6	77.1 ± 4.3	90.4 ± 2.1
1000	104.8 ± 28.4	48.6 ± 8.2	97.4 ± 10.6

Effect of MU on HA Synthesis and Chain Elongation in a Cell-free HA Synthesis System—Cell-free HA synthesis was examined by using the membrane-rich fraction of 3Y1-HAS2 cells. As shown in Fig. 2*A*, HAS activity was inhibited by MU in a dose-dependent manner, and the inhibition reached to 50% of the nontreated control at 300 μM MU. The inhibitory effect was observed at an early stage of HA synthesis and reached a plateau 30 min after treatment with MU (Fig. 2*B*). The size distribution of HA synthesized in the cell-free system was also determined by agarose gel electrophoresis (Fig. 2, *C* and *D*). The decrease in the molecular size of HA was caused by MU treatment in both a dose- and time-dependent manner. These data suggest MU inhibits HA synthesis by suppressing HAS function post-transcriptionally. Furthermore, the MU-mediated inhibition of HA synthesis may be caused by direct inhibition of HAS activity.

MU has been used as a substrate to measure the activity of UGTs, which are involved in the detoxification of phenolic

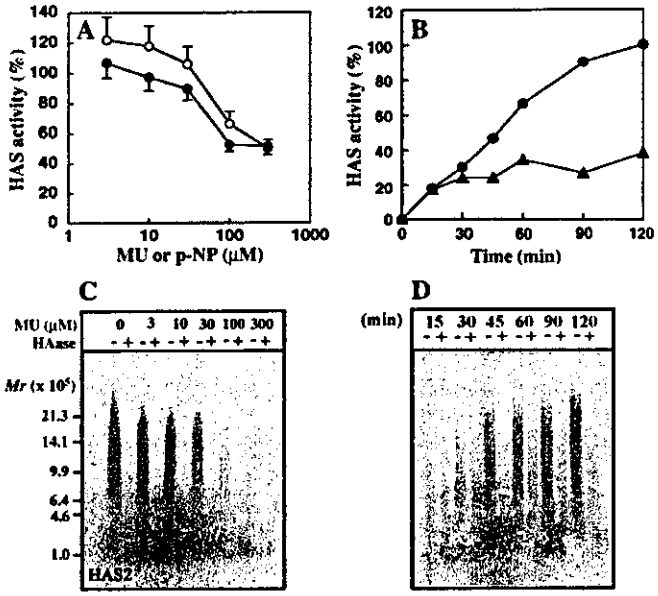

FIG. 2. **Effects of MU or *p*NP on HAS activity and size distribution of synthesized HA.** *A*, membrane-rich fraction from 3Y1-HAS2 cells was incubated with various concentrations of MU (*closed circles*) or *p*NP (*open circles*), and then HAS activity was calculated as a percentage relative to that of the nontreated sample. *B*, HAS activities were measured at various periods after the treatment of 3Y1-HAS2 transfectants without (*closed circles*) or with 300 μM MU (*closed triangles*). *C*, the same reaction supernatants were digested with (+) or without (−) 10 turbidity reducing units of *Streptomyces* hyaluronidase, and the size distributions of HA were then analyzed by 0.5% agarose gel electrophoresis. Radiolabeled HA was detected by autoradiography. Standard HA samples with known molecular size were used to determine the size distributions of newly synthesized HA. *D*, the time-dependent effect of MU on the chain elongation was assessed as above. *Plus* and *minus* indicate samples treated with or without 300 μM MU, respectively.

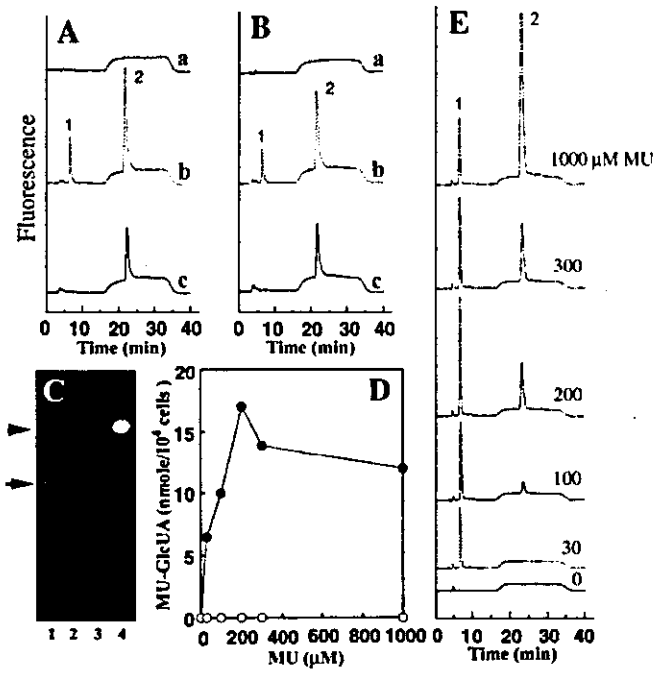

FIG. 3. **HPLC and TLC analyses of MU derivatives found in the culture conditioned medium.** 3Y1-HAS2 (*A*) and 3Y1-Mock (*B*) cells were incubated without (*a*) or with 1000 μM MU (*b* and *c*) for 24 h. The conditioned medium was analyzed before (*a* and *b*) and after digestion (*c*) with 1 unit of β-glucuronidase by HPLC on TSK gel ODS 120-T. *Peaks 1* and *2* corresponded to MU-GlcUA and MU used as authentic standards, respectively. *C*, peak 1 in the HPLC, with a retention time coinciding with that of an authentic MU-GlcUA standard, was collected and analyzed by TLC. *Lane 1*, standard MU-GlcUA; *lane 2*, peak 1 from 3Y1-HAS2 cells; *lane 3*, peak 1 from 3Y1-Mock cells; *lane 4*, standard MU. *D*, 3Y1-HAS2 cells were treated with various concentrations of MU for 24 h, and the production amounts of peak 1 in the conditioned medium (*closed circle*) and in the cell lysate (*open circle*) were expressed per viable cell number. *E*, HPLC profiles of MU derivatives from 3Y1-HAS2 cells treated with various concentrations of MU for 24 h.

compounds in mammalian cells, particularly in the liver (38). Because HAS possesses a glycosyltransferase activity for UDP-GlcUA within its polypeptide (17), we initially hypothesized that the enzyme is able to transfer GlcUA to MU from UDP-GlcUA, and the glucuronidation of MU competitively inhibits chain elongation of HA. We therefore tested the effect of *p*NP, another acceptor for UGTs (39), on HAS activity. As shown in Fig. 2*A*, HAS activity was indeed inhibited by *p*NP.

Production of MU-GlcUA in the Culture Medium and in the Reaction Supernatant of the Cell-free HA Synthesis—The effects of both MU and *p*NP prompted us to investigate whether the glucuronidation of these compounds is involved in the inhibition of HAS activity. The production of MU-GlcUA was analyzed by HPLC by using conditioned medium from 3Y1-HAS2 and 3Y1-Mock cells which were cultured for 24 h in the presence of various concentrations of MU. In the presence of MU, two major peaks appeared with a retention time of ~7 and 22 min (Fig. 3, *A* and *B*). The peak 2 at 22 min corresponded to that of the MU standard, whereas the peak 1 at 7 min was identified as MU-GlcUA because this coincided with that of an authentic standard sample and was sensitive to treatment with β-glucuronidase. Interestingly, a similar level of MU glucuronidation was observed in the control 3Y1-Mock cells (Fig. 3*B*) which express low levels of endogenous HAS2 and HAS3. This suggests that glucuronidation was mediated by the endogenous UGT activity expressed in the 3Y1 host cells. The MU derivative in peak 1, collected from the HPLC fraction, migrated on TLC at the same position as authentic standard MU-GlcUA (Fig. 3*C*). To estimate the molecular weight of the MU derivative, the peak 1 observed on HPLC was collected and subjected to mass spectrometry. The negative ion mass spectrum of the peak 1 from 3Y1-HAS2, shown in Fig. 4, had a $[M - H]^-$ ion peak at *m/z* 351. Therefore, the molecular weight of the MU derivative in peak 1 was determined to be 352, which was consistent with the calculated mass for MU-GlcUA ($C_{16}H_{16}O_9$; M_r = 352). The molecular ion at *m/z* 351 was also determined when the peak 1 from 3Y1-mock was used. The combined results of HPLC, TLC, and mass spectrometry confirmed that the MU derivative in peak 1 is MU-GlcUA (chemical structure is shown in Fig. 4). When 3Y1-HAS2 cells were cultured with various concentrations of MU, maximal production of MU-GlcUA was observed at 200 μM of MU (Fig. 3, *D* and *E*) both in the culture-conditioned medium and in the cell lysate. Most MU-GlcUA was secreted into the culture medium (Fig. 3*D*). The production of MU-GlcUA in the cell lysate was 60 fmol/10^4 cells at 200 μM of MU, which was much less than that in the culture conditioned medium, 17.0 nmol/10^4 cells. The secretion may be mediated by ATP-binding cassette transporters of the multidrug resistance protein family as demonstrated in the other cell systems (40). It was difficult to estimate the ratio of the UDP-GlcUA consumed for production of MU-GlcUA to total intracellular UDP-GlcUA. It seems, however, reasonable to assume that the amount of UDP-GlcUA, which had been consumed to produce MU-GlcUA, is equal to (or more than) the amount of the produced MU-GlcUA. Total amounts of secreted and intracellular MU-GlcUA suggested that 22.8 and 9.4% of loaded MU was converted to MU-GlcUA at the concentrations of 30 and 300 μM, respectively.

Transglycosylation of GlcUA to MU or *p*NP was confirmed by TLC analysis of the cell-free reaction mixture. When UDP-

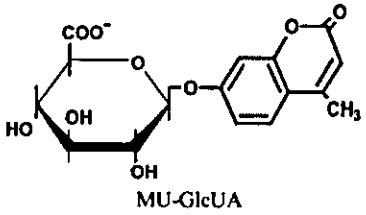

MU-GlcUA

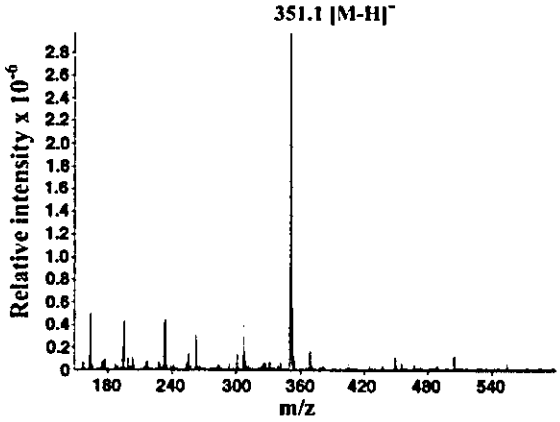

FIG. 4. **Chemical structure of MU-GlcUA and mass spectrum of MU derivative.** Peak 1 from 3Y1-HAS2, eluted at the same position of authentic standard MU-GlcUA in the HPLC (Fig. 3), was collected and analyzed by mass spectrometry. The conditions were described under "Experimental Procedures."

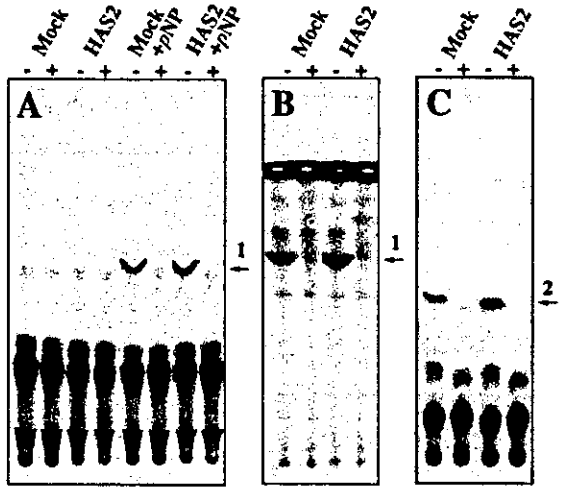

FIG. 5. **TLC analysis of *p*NP- or MU-GlcUA produced in the supernatant of the cell-free HA synthesis.** The membrane-rich fractions from 3Y1-Mock or 3Y1-HAS2 cells were incubated in the presence of UDP-[^{14}C]GlcUA and *p*NP (*A*), or UDP-GlcUA and [^{14}C]*p*NP (*B*), or UDP-[^{14}C]GlcUA and MU (*C*), and the reaction supernatants were analyzed by TLC on a Silica 60 plate as described under "Experimental Procedures." *Arrow 1* and *2* show the positions corresponding to those of the standard *p*NP- or MU-GlcUA, respectively. *Minus* and *plus* show samples before and after treatment with 2 units of β-glucuronidase.

[^{14}C]GlcUA was used to monitor the glucuronidation, radiolabeled spots corresponding to authentic MU-GlcUA or *p*NP-GlcUA used as standards were produced by endogenous UGTs in the presence of MU or *p*NP, respectively (Fig. 5, *A* and *C*). When UDP-GlcUA and [^{14}C]*p*NP were added to the cell-free HA synthesis, radiolabeled spots corresponding to *p*NP-GlcUA were also detected on TLC (Fig. 5*B*). The radiolabeled spots disappeared after treatment with β-glucuronidase, showing that GlcUA was transferred from UDP-GlcUA to MU or *p*NP in the cell-free HA synthesis. Our experiments suggest that HAS does not mediate the glucuronidation of MU or *p*NP, because MU-GlcUA and *p*NP-GlcUA were detected using both 3Y1-HAS2 and 3Y1-Mock cells.

Effect of MU-GlcUA on the HAS Activity—MU and *p*NP derivatives of xylosides, MU-Xyl and *p*NP-Xyl, have been shown to act as artificial primers for the initiation of glycosaminoglycan synthesis in cultured mammalian cells (41, 42). These derivatives behave as native primers. We then considered the possibility that MU-GlcUA and *p*NP-GlcUA might affect the initial step in HA elongation. To examine this possibility, MU-GlcUA or *p*NP-GlcUA was added to the cell-free HA synthesis. As expected, HAS activity was inhibited by MU-GlcUA or *p*NP-GlcUA in a dose-dependent manner (Fig. 6, *A* and *B*). However, the inhibitory activity of these compounds was far less than that of aglycon, MU, and *p*NP, suggesting that they do not directly inhibit HA synthesis. Surprisingly, similar results were also obtained using other sugar derivatives of MU or *p*NP, *i.e.* MU-GlcNAc, MU-Glc, *p*NP-GlcNAc, and *p*NP-Glc. Indeed when any of the *p*NP sugar derivatives were incubated with UDP-[^{14}C]GlcUA in the cell-free HA system, the *de novo* production of radiolabeled *p*NP-GlcUA was detected by TLC (Fig. 6*C*). However, radiolabeled *p*NP-GlcUA was absent when the *p*NP sugar derivatives were incubated without the membrane fraction (data not shown). The *de novo* production of radiolabeled *p*NP-GlcUA could be due to the liberation of *p*NP or MU from its respective sugar derivative and the transfer of GlcUA to the free aglycon from UDP-GlcUA by the endogenous UGT activity. Therefore, the inhibition of HAS activity may be dependent on the repeated glucuronidation of the free aglycon liberated from the sugar derivatives.

UGTs Enhanced the Inhibition of HAS Activity by MU—Although our results suggested that MU-GlcUA did not directly inhibit HAS activity, the production of MU-GlcUA by the endogenous UGTs seemed to be important for inhibition. We therefore investigated whether the inhibitory effect of MU and *p*NP was related to glucuronidation. To test this hypothesis, we examined the effect of recombinant UGT proteins on the inhibition by MU or *p*NP. Increased glucuronidation of *p*NP was observed by TLC when a recombinant UGT1A6 protein was added to the reaction mixture of cell-free HA synthesis (Fig. 7*B*). Under the same conditions used in the TLC analysis, the recombinant UGT significantly enhanced the inhibitory effect of *p*NP on HA synthesis (Fig. 7*A*). In contrast, UGT did not affect the HAS activity in the absence of *p*NP regardless of whether it was active or not. Almost the same degree of inhibition was observed by adding UGT1A7, which is one of the isoforms, in the presence of *p*NP or MU (Fig. 7*C*). These results suggested that the inhibition of HAS activity was directly related to extent of glucuronidation mediated by UGT.

The link between the inhibition of HAS and glucuronidation was further confirmed using the transfectants overexpressing a human UGT1A6 isoform (Fig. 8). The UGT1A6 and/or HAS2 expression plasmids were transiently transfected into COS cells, and the HAS activity was then measured in the presence or absence of 100 μM MU. COS cells do not express any UGT activity, as only a trace amount of MU-GlcUA was detected by TLC in the case of the membrane-rich fraction from the Mock or HAS2 transfectants (Fig. 8*B*). However, a large amount of MU-GlcUA was detected when UGT1A6 was expressed in the COS cells (Fig. 8*B*). The system is therefore suitable for investigating the effects of MU glucuronidation on the HAS activity. When COS cells co-transfected with both UGT1A6 and HAS2 cDNA were treated with MU, HAS activity was only 30% that of the untreated control value (Fig. 8*A*). However, for the membrane-rich fraction from transfectants expressing HAS2 alone, only a slight decrease in HAS activity was observed in the

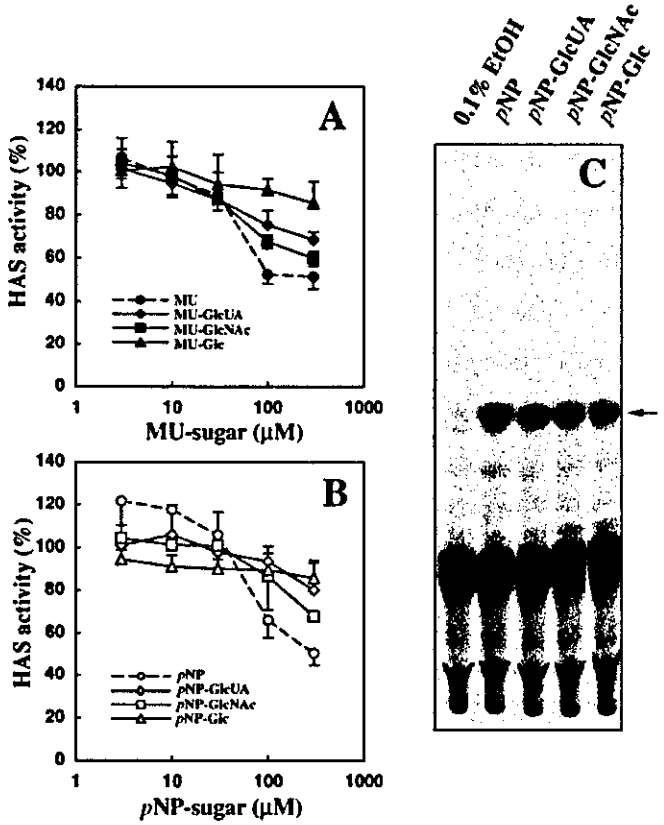

FIG. 6. **Effects of MU- and *p*NP-sugars on HAS activity.** The effects of various sugar derivatives of MU (*A*) or *p*NP (*B*) were assessed by cell-free HA synthesis. Various concentrations of MU (*closed circles*), MU-GlcUA (*closed diamonds*), MU-GlcNAc (*closed squares*), MU-Glc (*closed triangles*), *p*NP (*open circles*), *p*NP GlcUA (*open diamonds*), *p*NP-GlcNAc (*open squares*), and *p*NP-Glc (*open triangles*) were added in the membrane-rich fractions prepared from HAS2 transfectants, and then the HAS activities were calculated as percentages relative to that of the nontreated sample. Data represent average of three independent experiments ± S.D. *C*, membrane-rich fractions from 3Y1-HAS2 cells were incubated with 100 μM *p*NP-sugars and UDP-[^{14}C] GlcUA, and the production of *p*NP-GlcUA was analyzed on TLC. Radiolabeled spots corresponding *p*NP-GlcUA (*arrow*) were detected by autoradiography.

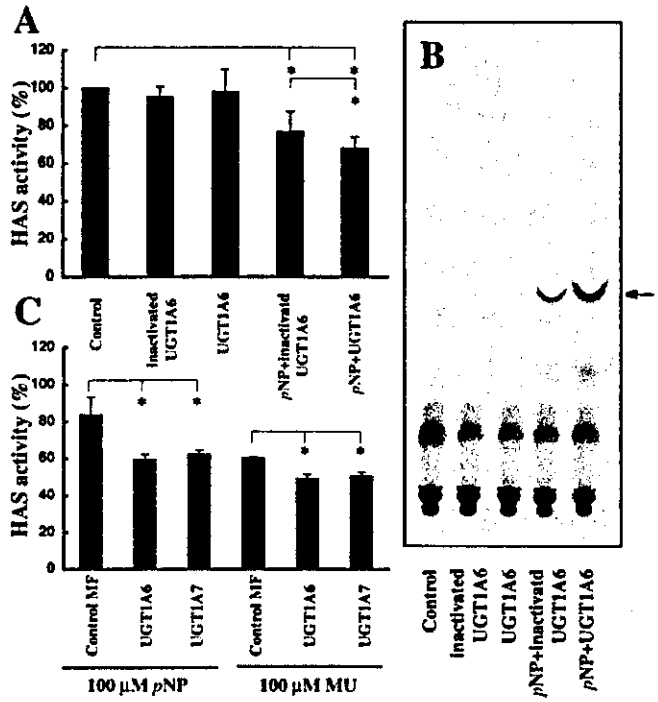

FIG. 7. **Enhanced inhibition of HAS activity by recombinant UGT proteins.** *A*, partially purified recombinant human UGT1A6 was added together with 100 μM *p*NP in the cell-free HA synthesis, and then the HAS activities were calculated as percentages relative to the nontreated sample. Inactivated UGT1A6 was obtained by boiling the active enzyme. Data represent average of three independent experiments ± S.D. *, $p < 0.05$. *B*, membrane fractions from 3Y1-HAS2 cells were incubated with 100 μM *p*NP and UDP-[^{14}C]GlcUA, and the production of *p*NP-GlcUA was analyzed on TLC. Radiolabeled spots corresponding *p*NP-GlcUA (*arrow*) was detected by autoradiography. *C*, partially purified UGT1A6 or UGT1A7 was added together with 100 μM *p*NP or MU in the cell-free HA synthesis system, and then the HAS activities were calculated as percentages relative to the nontreated sample. Membrane fractions prepared from insect cells infected with baculovirus vector alone were used as a control membrane fractions. Data represent average of three independent experiments ± S.D. *, $p < 0.05$.

presence of MU (Fig. 8*A*). HA production into the conditioned medium was also measured when these transfectants were cultured with or without MU. The results were similar to those obtained using the cell-free system (Fig. 8*C*). Taken together, these results suggest that the inhibition of HA synthesis by MU or *p*NP is caused by the UGT-dependent glucuronidation of these compounds.

Effect of UDP-GlcUA on the Inhibition of HAS Activity by MU—The inhibition of HA synthesis may be caused by a depletion in the pool of UDP-GlcUA due to UGT-mediated MU glucuronidation. If this hypothesis is correct, we would expect HAS activity to recover after addition of an excess amount of UDP-GlcUA to the cell-free HA synthesis, even in the presence of MU. Indeed, we did observe the recovery of HAS activity following addition of UDP-GlcUA in a dose-dependent manner (Fig. 9*A*). UDP-GlcUA was then added to the reaction mixture 1 h after the initiation of HA synthesis. The HAS activity inhibited by the MU treatment was partially rescued when the UDP-GlcUA concentration increased (Fig. 9*B*). We also determined whether HAS inhibition was enhanced by pretreatment of the membrane fraction with MU prior to the initiation of the HA synthesis. If the kinetic lag shown in Fig. 2*B* reflects the duration for the depletion of UDP-GlcUA in the reaction mixture or formation of MU derivative inhibitor, then the preincubation would inhibit HAS activity more completely. However, time-dependent changes in the HAS activity revealed that the kinetic lag still remained, and the effect was minimal at an early incubation time (Fig. 10). Furthermore, the pretreatment of membranes with MU-GlcUA had a lesser effect on HAS activity than that of MU (Fig. 10), suggesting that the HAS activity is not inhibited irreversibly by MU-GlcUA. This was also confirmed by the experiment where HAS activity was measured under the MU-GlcUA-free conditions using membrane fractions pretreated with 300 μM MU-GlcUA (data not shown). A similar result was also obtained when the membrane fractions were pretreated with 300 μM MU (data not shown). Taken together, the results suggest that the glucuronidation event followed by the subsequent reduction of UDP-GlcUA concentration affects the HAS activity at the late stage of HA elongation.

DISCUSSION

In this study we present a novel mechanism for the inhibition of HA synthesis involving the UGT-dependent glucuronidation of MU. Although MU has been widely used as an inhibitor of HA synthesis (10, 25, 26), the exact inhibitory mechanism is not clear, especially in mammalian cells. A major problem in the elucidation of this inhibitory mechanism has been the complexity of the HA synthetic system that is regulated by three related mammalian HAS isoforms, HAS1, HAS2, and HAS3 (17). To reduce this complexity we initially established three rat 3Y1 cell lines, each expressing a distinct HAS isoform, to test whether MU inhibited HA production and ma-

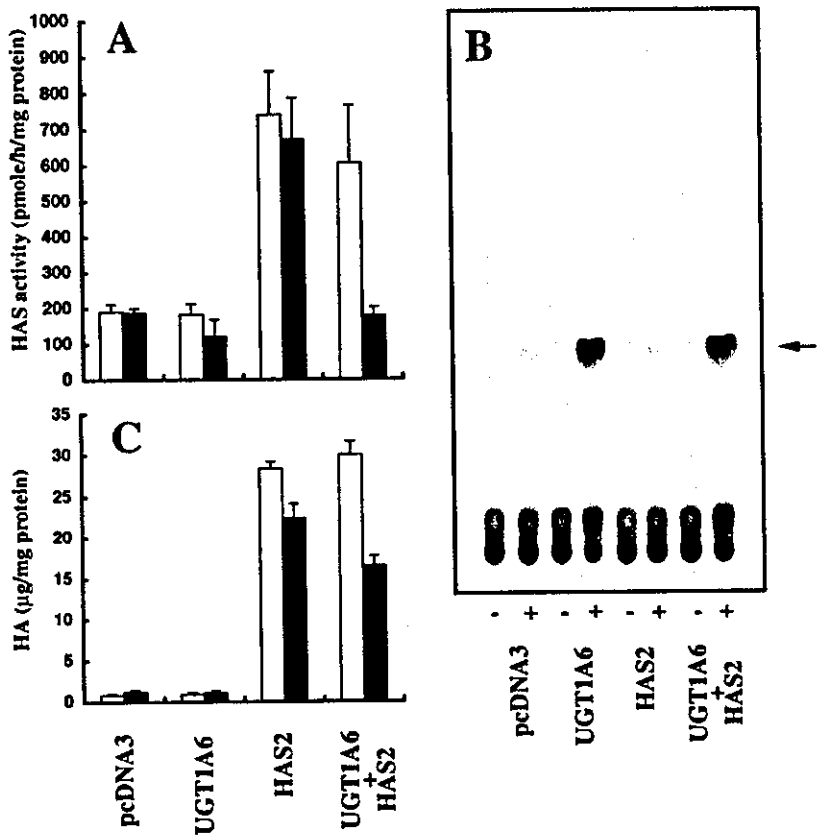

FIG. 8. **Overexpression of human UGT1A6 enhanced the inhibition of HAS activity and HA synthesis by MU.** *A*, membrane-rich fractions from COS transfectants expressing UGT1A6 and/or HAS2 were incubated with (*solid bars*) or without (*open bars*) 100 μM MU, and the HAS activities were then calculated as percentages relative to the control. *B*, membrane-rich fractions from COS transfectants were incubated without or with 100 μM MU and UDP-[^{14}C]GlcUA, and the production of MU-GlcUA was analyzed on TLC. Radiolabeled spots corresponding to MU-GlcUA (*arrow*) were detected by autoradiography. *Plus* and *minus* indicate samples in the presence or absence of MU, respectively. *C*, the HA contents in the conditioned medium of COS transfectants expressing UGT1A6 and/or HAS2 were measured by ELISA-like assay 24 h after the treatment with (*solid bars*) or without (*open bars*) 300 μM MU. Data represent average of three independent experiments ± S.D.

trix formation in a similar way to that observed for human skin fibroblasts (23, 24). When the cells were cultured in the presence of MU, a decrease in both HA production and matrix formation was observed in all three transfectants, and in particular the HAS2 transfectant (data not shown). Therefore, we adopted HAS2 expressing cells to further elucidate the inhibition mechanism of MU in this study.

We had observed previously growth suppression of human skin fibroblasts when treated with a high concentration of MU. HA synthesis is known to be down-regulated in growth-arrested cells (43). Our recent study (44) also suggested that HAS gene expression is regulated via signaling cascades linked to cell proliferation. Therefore, we investigated whether the antiproliferative effect of MU lowers the expression of HAS and subsequently HA synthesis. At low and moderate concentrations of MU, however, we could not detect any significant change in the transcriptional levels of endogenous HAS genes in the rat 3Y1 transfectants, despite the significant decrease in HA synthesis. The fact that MU inhibited HA synthesis, even in the transfectants in which HAS expression is driven by an exogenous promoter, suggested the post-transcriptional inhibition of HA synthesis. However, we could not rule out the possibility that MU down-regulated the promoter activity of the endogenous HAS genes because they were moderately suppressed at high concentrations of MU.

To avoid the influence of growth suppression, we examined the effect of MU on HAS activity in a cell-free system. The HAS activity in the crude membrane fraction from the HAS2 transfectants was inhibited by MU treatment. The result is consistent with the idea that MU inhibits HA synthesis post-transcriptionally and in a growth-independent fashion. Interestingly, a similar result was obtained when *p*NP was tested for the ability to inhibit HAS activity in the cell-free HA synthesis. This led us to examine whether these two compounds, known to be good substrates for UGT, can act as acceptors for glucuronyltransferase of HAS. A substantial amount of glucuronidation of MU was observed in the conditioned medium and in the supernatant of the cell-free HA synthesis. Intriguingly, a considerable amount of glucuronidation was also observed in the control cells expressing very little HAS, suggesting that MU was glucuronidated by an endogenous UGT other than HAS. Monosaccharide derivatives of MU and *p*NP have been shown to act as artificial primers for the initiation of glycosaminoglycan biosynthesis in cultured mammalian cells (41, 42). In plants, the lipid-sugar conjugate has been shown to act as a primer in the synthesis of cellulose (45). We considered the possibility that MU-GlcUA may act as an artificial initiation primer for HA synthesis thereby decreasing the efficiency of HA polymerization, the primary role of HAS. However, this hypothesis seemed unlikely because the inhibition rate of MU-GlcUA was less than that of MU. Moreover, no elongation products of MU-GlcUA were detected in the conditioned medium or in the supernatant of the cell-free HA synthesis (data not shown). Alternatively, previous studies (23, 46) have shown that MU and *p*NP derivatives of xylosides, MU-Xyl and *p*NP-Xyl, significantly inhibited the biosynthesis of HA as well as sulfated glycosaminoglycans. As for the mechanism, it was suggested that free *p*NP, which is generated by the enzymatic hydrolysis of *p*NP-Xyl, mediated the inhibitory effect (47). In the current study, we also detected a significant liberation of *p*NP from its sugar derivatives. These results together with our finding that glucuronidation of the free aglycons occurred in parallel with the increased inhibition rate of HA synthesis support the importance of the glucuronidation in the inhibition.

Elevating the level of MU-GlcUA, by addition of exogenous recombinant UGT, promoted the inhibition of HA synthesis in the cell-free system. Furthermore, when COS cells overexpressing UGT and HAS2 were treated with MU, the inhibitory effects were enhanced both in terms of HAS activity and HA production. Excess glucuronidation of MU by UGT could deplete the pool of UDP-GlcUA, which is a common substrate for HAS and UGT. As shown in Fig. 9*A*, the inhibition of HA

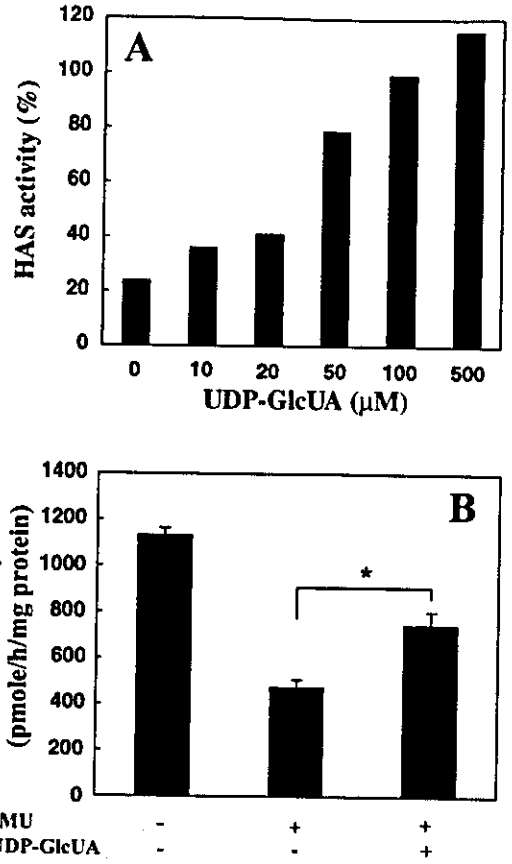

FIG. 9. **Excess amount of UDP-GlcUA diminished the effect of MU on HAS activity.** *A*, various concentrations of UDP-GlcUA were added together with 100 μM MU in the membrane-rich fractions from COS transfectants co-expressing UGT1A6 and HAS2, and the HAS activities were then calculated as percentages relative to that of the nontreated sample. The inhibitory effect of MU was diminished to the control level by an excess amount of UDP-GlcUA. *B*, the membrane-rich fractions from COS transfectants co-expressing UGT1A6 and HAS2 were preincubated for 1 h with (+) or without (−) 300 μM MU in the reaction buffer as described under "Experimental Procedures." Additional UDP-GlcUA was then supplied at the concentration of 0.1 mM to the reaction mixture and further incubated at 37 °C for 1 h. The inhibition of HAS after treatment with MU was partially rescued at the increased concentrations of UDP-GlcUA. Data represent average of three independent experiments ± S.D. *, $p < 0.05$.

synthesis was reduced to the control level when an excess of UDP-GlcUA was added to the *in vitro* reaction mixture. Thus, it is conceivable that the cellular concentration of UDP-GlcUA could be an important factor in the inhibitory action of MU. To clarify the mode of action, we determined whether the HAS inhibition was enhanced by pretreatment of the membrane fraction with MU or MU-GlcUA prior to initiating HA synthesis. Time-dependent changes in HAS activity demonstrated that pretreatment with MU exerted little effect on the inhibition of HA synthesis at the initiation step (Fig. 10). However, the inhibition of HAS activity after MU treatment was partially rescued by increasing the UDP-GlcUA concentration at the later time points (Fig. 9*B*). Taken together, the results suggest that the glucuronidation event followed by the subsequent reduction of UDP-GlcUA concentration predominantly affects the chain elongation after the lag period of HAS inhibition. Consistent with this idea, the chain elongation of HA was reduced by MU after the lag period as shown in Fig. 2. This could be rationalized by assuming that the K_m value for UDP-GlcUA of HAS enzymes is altered in a manner depending on the chain length of synthesizing HA.

The glucuronidation event may affect HAS activity to a greater extent in the cells expressing elevated levels of UGTs.

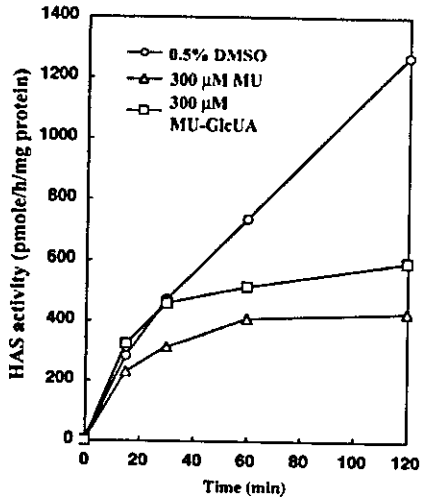

FIG. 10. **Pretreatment of the membrane fractions with MU or MU-GlcUA.** The membrane fractions isolated from 3Y1-HAS2 transfectants were preincubated for 1 h with 0.1 mM UDP-GlcUA in the presence of 300 μM MU or MU-GlcUA. The HA synthesis was then initiated by addition of a saturated concentration of UDP-GlcNAc, and time-dependent changes in the HAS activity were monitored by the incorporation of radioactivity into the HA fraction. A slight inhibition of HAS activity was observed at 15 min and became more apparent thereafter. The effect of MU-GlcUA was less than that of MU itself. Data represent average of two independent experiments.

Indeed, MU significantly lowered HAS activity in rat 3Y1 cells expressing endogenous UGT, in contrast to COS cells that do not express any UGT. Altering the cellular level of UDP-GlcUA would be expected to mirror these observations. Depletion of UDP-GlcUA in the cellular pools may affect the biosynthesis of other GlcUA-containing glycosaminoglycans such as heparan sulfate and chondroitin sulfate. Previous studies, however, indicated that the action of MU had no affect on glycosaminoglycan biosynthesis in human skin fibroblasts (23, 24). We considered several possible explanations related to the selective inhibition of the synthesis by MU. MU may specifically target HAS due to its cellular localization, which is different from other glycosyltransferases, exostosin (EXT) family (48, 49) and chondroitin synthases (50–52) involved in the biosynthesis of heparan sulfate and chondroitin sulfate, respectively. All the glycosaminoglycans, with the single exception of HA, are synthesized at the intracellular Golgi network. HA is synthesized on the inner side of the plasma membrane by a membrane-associated HAS (17). The cell-free HA synthesis revealed that UGT activity is present in the membrane preparations. This is consistent with previous observations (53) in which most UGTs are present in the endoplasmic reticulum and nuclear membrane. Glucuronidation of MU may result in a differential reduction in the local concentration of UDP-GlcUA near the plasma membrane and in the Golgi and endoplasmic reticulum. Alternatively, this observation could be rationalized by assuming that the K_m value for UDP-GlcUA of these enzymes varies markedly. In previous work, however, the K_m values for UDP-GlcUA were similar among recombinant HAS2 (32), chondroitin synthases (51, 52), and UGT1A6 (54). Another explanation for the selective inhibition would be the preferential effects of MU on the chain elongation of a large molecular mass of HA (over 1×10^6 Da) as shown in Fig. 2.

One might expect a common inhibition mechanism for MU in both the mammalian cells and *Streptococcus*, because they synthesize HA with exactly the same structure by using homologous enzymes (17). A possibility of the post-transcriptional inhibitory mechanism was also speculated from the results in group C *Streptococcus* that MU did not affect the expression level of HAS (28). On the other hand, we speculated that MU